PARIS, an optogenetic method for functionally mapping gap junctions

Ling Wu[1,2,3], Ao Dong[1,2,3], Liting DONG[1,2,3], Shi-Qiang Wang[1], Yulong Li[1,2,3*]

[1]State Key Laboratory of Membrane Biology, Peking University School of Life Sciences, Beijing 100871, China

[2]PKU-IDG/McGovern Institute for Brain Research, Beijing 100871, China

[3]Peking-Tsinghua Center for Life Sciences, Beijing 100871, China

*Correspondence: yulongli@pku.edu.cn

ABSTRACT

Cell-cell communication via gap junctions regulates a wide range of physiological processes by enabling the direct intercellular electrical and chemical coupling. However, the *in vivo* distribution and function of gap junctions remain poorly understood, partly due to the lack of non-invasive tools with both cell-type specificity and high spatiotemporal resolution. Here we developed PARIS (pairing actuators and receivers to optically isolate gap junctions), a new fully genetically encoded tool for measuring the cell-specific gap junctional coupling (GJC). PARIS successfully enabled monitoring of GJC in several cultured cell lines under physiologically relevant conditions and in distinct genetically defined neurons in *Drosophila* brain, with ~10-sec temporal resolution and sub-cellular spatial resolution. These results demonstrate that PARIS is a robust, highly sensitive tool for mapping functional gap junctions and study their regulation in both health and disease.

INTRODUCTION

Gap junctions are intercellular channels that are expressed in virtually all tissue

1

26 types in both vertebrates and invertebrates. They allow direct transfer of small

27 molecules such as ions, metabolites and second messengers between

28 connected cells, thereby playing essential roles in various physiological

29 processes, including embryo development, metabolic coordination of avascular

30 organs, tissue homeostasis and synchronizing electrical activity in excitable

31 tissues (Bennett and Zukin, 2004; Kumar and Gilula, 1996). Defects of gap

32 junction function are linked with a wide array of diseases, including myocardial

33 infarction, hearing loss and hypomyelinating disorder (Jongsma and Wilders,

34 2000; Laird, 2010; Sohl et al., 2005). Studying gap junction coupling (GJC)

35 under physiological or disease conditions in complex systems such as the

36 nervous system requires a non-invasive method with both cell-type specificity

37 and high spatiotemporal resolution. Current methods used to monitor GJC

38 include paired electrophysiological recordings (Bennett et al., 1963; Furshpan

39 and Potter, 1959), dye microinjection (Stewart, 1978), fluorescence recovery

40 after photobleaching (FRAP) (Wade et al., 1986), and local activation of

41 molecular fluorescent probes (LAMP) (Dakin et al., 2005), all of which are either

42 invasive and/or lack cell-type specificity, thus limiting their use in heterogeneous

43 tissues. Recently, hybrid approaches have been developed in which genetically

44 encoded hydrolytic enzymes or promiscuous transporters are used to introduce

45 small molecule substrates or peptides tagged with a fluorescent label in specific

46 cells (Qiao and Sanes, 2015; Tian et al., 2012). Although these methods might

47 provide cell type specific investigation of GJC, the requirement of exogenous

48 substrate and the background generated by endogenous enzymes or

49 transporters still make them difficult to apply *in vivo*. In addition, dye diffusion is

50 an irreversible process and thus these methods are difficult to be applied to

51 examine the same gap junctions repeatedly in order to measure their dynamics,

52 regulations and plasticity (Dong et al., 2018).

53 To overcome these limitations, we developed an all-optical approach named

54 PARIS (pairing actuators and receivers to optically isolate gap junctions) in

2

55 which we express an optically-controlled actuator in one cell, to generate an

56 electrochemical gradient of specific molecules between two connected cells,

57 and a fluorescent receiver in the adjacent cell, to detect the movement of the

58 molecules across the gap junctions. GJC between the actuator cell (i.e.,

59 expressing actuators) and the receiver cell (i.e., expressing receivers) is

60 detected by a fluorescence increase in the receiver followed by the optical

61 activation of the actuator (Figure 1A).

62 **RESULTS**

63 **Development of a novel all-optical tool for monitoring GJC**

64 At the beginning, we tested several pairs of optical actuators/receivers based

65 on generating/detecting small molecules that can readily diffuse across gap

66 junctions, such as cGMP, Ca^{2+} and proton (H^+). Our first step was to test

67 whether the actuator/receiver pair can generate a cell-autonomous signal. We

68 found that, when co-expressed in HEK293T cells (i.e., in the *cis* configuration),

69 neither a light-activated cGMP cyclase BeCylOp (Gao et al., 2015) paired with

70 a cGMP sensor FlincG3 (Bhargava et al., 2013) nor the red shifted

71 channelrhodopsin CsChrimson (Klapoetke et al., 2014) paired with a sensitive

72 Ca^{2+} indicator GCamP6s (Chen et al., 2013) could generate detectable light-

73 induced signal (Figure 1 - figure supplement 1).

74 Interestingly, when we co-expressed a light-gated outward proton pump ArchT

75 (Han et al., 2011) and a pH-sensitive green fluorescent protein pHluorin

76 (Miesenbock et al., 1998; Sankaranarayanan et al., 2000) in HEK293T cells, a

77 4-sec laser illumination at 561 nm elicited a robust increase in pHluorin

78 fluorescence, with the membrane-targeted pHluorin (pHluorinCAAX) producing

79 a larger change in fluorescence than the cytosolic pHluorin (Figure 1 - figure

80 supplement 2A,B). No light-induced change in fluorescence was observed in

81 cells that co-expressing pHluorinCAAX and the deficient proton-pump

82 ArchTD95N (Kralj et al., 2012), or in cells that only express pHluorinCAAX

3

83 (Figure 1 - figure supplement 2A,B). Furthermore, the evoked response is

84 dependent on both the duration and the power of the activating light (Figure 1 -

85 figure supplement 2C-F). These results demonstrate that ArchT and pHluorin

86 can function as a pair of proton actuator and proton sensor.

87 We next examined whether PARIS based on ArchT/pHluorin can be used to

88 measure GJC between cultured HEK293T cells, which endogenously express

89 both connexin (Cx) 43 and Cx45, therefore spontaneously form gap junctions

90 between adjacent cells (Butterweck et al., 1994; Langlois et al., 2008). When

91 ArchT and pHluorin were separately expressed in neighboring cells (i.e., in

92 the *trans* configuration, see Methods; Figure 1B1), a brief photoactivation of

93 ArchT in the actuator cells (4 sec, ~0.5 mW, indicated by the yellow circle in

94 Figure 1B2) faithfully induced a ~4.3% $\Delta F/F_0$ increase in pHluorinCAAX

95 fluorescence in the neighboring receiver cells whereas non-adjacent

96 pHluorinCAAX-expressing cells had no measurable change in fluorescence

97 (Figure 1B2-3). Application of carbenoxolone (CBX, 100µM) which blocks gap

98 junctions (Connors, 2012) significantly decreased the light-induced PARIS

99 signal (Figure 1C), confirming that the signal measured in receiver cells is

100 mediated by GJC. Similar to autonomous signals, increasing the duration of

101 the illumination pulse from 1 sec to 20 sec incrementally increased the PARIS

102 response from ~2% to ~20% (Figure 1D-E). A 4-sec laser pulse was sufficient

103 to induce a robust PARIS signal (SNR = 23 ± 8, Figure 1F) with a half-rise

104 time of ~10 sec (Figure 1G). On the other hand, a 20-sec laser pulse induced

105 an ~4.3-fold increase in the signal-to-noise ratio compared to 4-sec with a half-

106 rise time of ~21 sec (Figure 1F,G); however, the half-decay time did not differ

107 between a 4-sec pulse and a 20-sec pulse ($t_{1/2\ decay}$ = 61 ± 5s and 67 ± 3s

108 respectively, Figure 1G). We also observed the spatially graded PARIS

109 signals in three receiver cells that are sequentially connected to the actuator

110 cell (Figure 1 - figure supplement 3). Specifically, the directly connected cell

111 had the strongest response, and the thirdly connected cell had the weakest

4

112   response (Figure 1 - figure supplement 3D).

113   We then quantified the ArchT-induced pH change in the actuator cells using the

114   ratiometric pH indicator mTagBFP-pHluorinCAAX generated by fusing the pH-

115   insensitive blue fluorescent protein mTagBFP(Subach et al., 2008) to the N-

116   terminus of pHluorinCAAX and then calibrating the correlation between pH and

117   the ratio of GFP/BFP fluorescence (Figure 1 - figure supplement 4). Based on

118   a fit to the titration curve, we estimated that a 4-sec and 20-sec laser pulse

119   induces a transient increase of intracellular pH from 7.35 to 7.45 and 7.80

120   respectively in actuator cells (Figure 1 - figure supplement 4D-F), which allowed

121   us to repeatedly elicit a PARIS signal in specific cells as shown above. Together,

122   these data provide proof-of-principle that PARIS is a robust tool for measuring

123   GJC between connected cells.

124   **Electrophysiological validation of PARIS and its comparison with FRAP**

125   **in HEK293T cells.**

126   We have showed that PARIS could detect GJC in a photostimulation dependent

127   way and sensitive to CBX (Figure 2A, D1 & Figure 1). Next, we further validated

128   PARIS by patch-clamping the receiver cell in order to record the gap junction–

129   mediated current induced by activating the actuator cell using a laser pulse

130   (Figure 2B1). Applying increasingly stronger light pulses to the actuator cell

131   yielded time-locked currents in the receiver cell that were blocked by CBX

132   (Figure 2B2,D2). In the same cells, voltage steps on the actuator cell also

133   elicited non-rectifying and CBX sensitive currents in the receiver cell (Figure

134   2C,D3). Quantification of the group data showed that the CBX inhibition of GJC

135   was independent from the approaches used to activate the actuator cell (by

136   light or voltage) and from the signals measured in the receiver cell

137   (pHluorinCAAX fluorescence or currents) (Figure 2E). In addition, we

138   performed a head-to-head comparison between PARIS and FRAP—a dye

139   diffusion based methods which detects the gap junction mediated fluorescence

5

140   recovery after photobleaching (Figure 2F). The PARIS signal was stable for five

141   sequential pulses at 2-min intervals, whereas the FRAP signal decayed

142   considerably over the same time period in terms of both basal fluorescence and

143   SNR (Figure 2G-I). Moreover, the PARIS signal had considerably faster kinetics

144   than FRAP, with a half-rise time of 21 sec compared to 197 sec, respectively

145   (Figure 2J).

146   **PARIS enables reporting regulations of gap junction and disease-causing**

147   **mutations in connexin genes.**

148   Phosphorylation has been implicated in the modulation of GJC by affecting the

149   trafficking, assembly/disassembly, degradation and gating of gap junctions

150   (Laird, 2005; Nihei et al., 2010) . To test whether PARIS could report GJC under

151   different regulations such as protein phosphorylation, we treated PARIS-

152   expressing HEK293T cells with the cAMP analog 8-Br-cAMP, the adenylyl

153   cyclase agonist forskolin, or the protein kinase C (PKC) agonist

154   tetradecanoylphorbol acetate (TPA). Compared with the control group, treating

155   cells with TPA significantly inhibited the PARIS signal compared to the control

156   group; in contrast, neither 8-Br-cAMP nor forskolin had obvious effect (Figure

157   3A, B), suggesting that activating PKC—but not protein kinase A—inhibits GJC,

158   which is in general consistent with previous reports (Lampe, 1994; Sirnes et al.,

159   2009).

160   Mutations in *GJA1*, the gene encoding Cx43, have been linked to a number of

161   diseases such as the inherited oculodentodigital dysplasia (Paznekas et al.,

162   2009). We therefore asked whether PARIS could be used to probe the function

163   of Cxs encoded by mutated Cx genes. We performed PARIS in HeLa cells,

164   which do not express measurable levels of endogenous Cxs (Elfgang et al.,

165   1995). As expected, no PARIS signal was elicited in receiver HeLa cells upon

166   photoactivating the actuator cell; while in HeLa cells expressing GJA1,

167   photoactivating the actuator cell elicited a robust fluorescence increase in the

6

168   adjacent receiver cell (Figure 3C,D). Interestingly, expressing a Cx43 protein

169   with either the R202H or R76H mutation—which affects Cx43 trafficking and

170   gap junction permeability (Shibayama et al., 2005)—caused a significant

171   reduction in the PARIS signal compared to cells expressing wild-type Cx43

172   (Figure 3C,D). These data indicate that PARIS can be used to probe the effects

173   of clinically relevant mutations in gap junction proteins.

174   **PARIS can report the activity of functional gap junctions between**

175   **cardiomyocytes**

176   Next, we examined whether PARIS can be used to study gap junctions in a

177   physiologically relevant system, namely cardiomyocytes (CMs). Gap junctions

178   formed by Cx40, Cx43, and Cx45 play an important role in CMs by

179   synchronizing their contractions and defects in these connexins have been

180   associated with cardiovascular diseases (Jongsma and Wilders, 2000). Using

181   CMs cultured from neonatal rats (Figure 3E), we observed that stimulating

182   actuator CMs induced a robust fluorescence increase in receiver CMs with half-

183   rise and half-decay times of approximately 14 and 21 sec respectively, and the

184   responses were reversibly blocked by the gap junction blocker heptanol

185   (Garcia-Dorado et al., 1997) (Figure. 3F-H). Neither the rate of spontaneous

186   Ca^{2+} transients in CMs nor the rate of cellular beating was altered by the

187   expression or stimulation of the actuator protein (Figure 3 - figure supplement

188   1), supporting the notion that expressing and activating PARIS does not affect

189   cellular functions.

190   **PARIS can be used to measure cell-specific GJC in *Drosophila* brain**

191   We then examined whether PARIS can be used to measure gap junction activity

192   (i.e., electrical synapses) between genetically defined cell types in the brain.

193   Using the *Drosophila* olfactory system as a model system, we first confirmed

194   that ArchT and pHluorin can produce cell-autonomous signals in an *ex vivo*

195   preparation (Figure 4 – figure supplement 1). We expressed both the actuator

7

196   and the receiver with dual binary expression systems (GH146-QF>QUAS-

197   ArchT, GH146-Gal4>UAS-pHluorinCAAX) in excitatory projection neurons

198   (ePNs) in the fly olfactory pathway (Stocker et al., 1997) and measured cell

199   autonomous PARIS signal from the antenna lobe (AL) in the isolated fly brain

200   (i.e., in the *cis* configuration, Figure 4 – figure supplement 1A-G). The ePN

201   autonomous signal could be elicited repeatedly in the same sample for up to

202   two hours, with no obvious loss of signal strength (Figure 4 – figure supplement

203   1H,I), indicating that PARIS is stable in intact living tissue.

204   We then used PARIS to measure electrical synapses formed between

205   excitatory projection neurons (ePNs) and excitatory local neurons (eLNs), both

206   of which have dendritic arborizations in the antennal lobe (AL) (Shang et al.,

207   2007) (Figure 4 – figure supplement 2, first row). We generated a transgenic

208   *Drosophila* line expressing the actuator (GH146-QF>QUAS-ArchT) selectively

209   in ePNs and the receiver (Kras-Gal4>UAS-pHluorinCAAX) selectively in eLNs

210   (Figure 4A). Stimulating a 20-μm diameter region in the AL elicited a rapid

211   increase in pHluorinCAAX fluorescence, with half-rise and half-decay times of

212   approximately 12 sec and 29 sec, respectively (Figure 4B,C,F,G), consistent

213   with previously reported electrophysiological data indicating that ePNs and

214   eLNs are electrically coupled (Huang et al., 2010; Yaksi and Wilson, 2010).

215   Importantly, no response was elicited in the brain when the transgenic flies were

216   pretreated with CBX or in the brain of *ShakB[2]* flies, which have a mutation in

217   their gap junction proteins (Zhang et al., 1999), confirming that the signal

218   measured in the receiver neurons is indeed mediated by gap junctions (Figure

219   4B,C,F,G). Next, we divided the AL into four regions based on orientation and

220   then scanned each region, revealing that laser illumination can induce a

221   fluorescence increase in each region (Figure 4D,E,H), indicating that electrical

222   coupling is a general property between ePNs and eLNs in the AL. In addition,

223   we examined gap junction activity between ePNs and other cell types by pairing

224   ePNs as the receiver cells with various actuator cells that have anatomical

8

225   overlap with ePNs, including inhibitory local neurons (iLNs), glial cells, and

226   Keyon cells (Figure 4 – figure supplement 2, second-bottom rows). However,

227   when activated, none of these three cell types caused a measurable PARIS

228   signal in the receiver cells (Figure 4 – figure supplement 3), suggesting that

229   ePNs may not form functional gap junction connections with iLNs, glial cells, or

230   Keyon cells.

231   **PARIS can be used to map functional gap junctions in distinct neuronal**

232   **structures**

233   Electrical coupling between neurons could happen through dendritic networks,

234   axon-axonal connections or somatic contacts, which contribute the signal

235   integration and decision of neuronal firing (Belousov and Fontes, 2013; Yaksi

236   and Wilson, 2010). Capitalizing on the entire optical nature of PARIS, we further

237   examined whether PARIS can be used to measure functional GJC in subcellular

238   compartments, thereby providing spatial resolution that is not accessible to

239   traditional methods such as electrophysiological recording or dye injection. In

240   the *Drosophila* olfactory system, ventrally localized inhibitory projection

241   neurons (iPNs) and ePNs form gap junctions participating odor information

242   processing (Wang et al., 2014). Anatomically, both ePNs and iPNs have

243   dendrites in the AL and axons that project to the lateral horn (LH) (Figure 6A,

244   B; see also Liang et al., 2013; Parnas et al., 2013). Thus, whether gap junctions

245   are formed between iPNs and ePNs in the AL, LH, or both is currently unknown.

246   To answer this question, we expressed the actuator (Mz699-Gal4>UAS-ArchT)

247   in iPNs and the receiver (GH146-QF>QUAS-pHluorinCAAX) in ePNs. We then

248   separately illuminated ePNs-iPNs overlapping regions in the AL or LH to test

249   the presence of functional GJC. Interestingly, stimulating the AL—but not the

250   LH—elicited a significant increase in pHluorinCAAX fluorescence, and this

251   response was eliminated in the presence of CBX (Figure 5B-D). As a control,

252   we confirmed that CBX had no significant influence on the autonomous signal

253   measured at either the AL or LH when both the actuator and receiver were co-

9

254   expressed in iPNs (i.e., in the *cis* configuration; Mz699>ArchT/pHluorin, Figure

255   5B, C, F). These results support the notion that iPNs and ePNs form functional

256   gap junctions at the AL (i.e., via dendrite-dendrite contacts), but not at the LH

257   (i.e., via axon-axon contacts).

258   **Further optimization of PARIS by screening of more potent proton pumps**

259   To further improve PARIS's performance for *in vivo* GJC detecting, we

260   explored the light sensitivity of proton pumps with high sequence homology to

261   ArchT cloned from fungi, algae, bacteria to proteobacteria (Figure 6A, up

262   right). By measuring the cell-autonomous pHluorin fluorescence increase in

263   response to green-yellow light, we found that five candidates exhibited larger

264     $\Delta F/F_0$ than ArchT with a fungi rhodopsin that we named Lari showed the best

265   membrane trafficking performance and 6-times the light-sensitivity of ArchT

266   (Figure 6A-C, Figure 6 – figure supplement 1). Therefore, Lari provides a

267   more powerful actuator for *in vivo* application of PARIS in the future.

268   **DISCUSSION**

269   Here, we developed a new tool named PARIS, an all-optical approach that can

270   facilitate mapping GJC in specific cells. We show that PARIS can be readily

271   adapted for use in both *in vitro* and *ex vivo* preparations, including cultured cell

272   lines, primary cardiomyocytes, and transgenic flies. We validated that this

273   system specifically reports functional gap junctions using a variety of

274   electrophysiological, pharmacological, and genetic approaches. By focusing on

275   defined sets of neurons in the *Drosophila* olfactory system, we show that as the

276   first completely genetically encoded method, PARIS can be applied to

277   repeatedly probe electrical synapses in distinct, genetically tractable neurons

278   with high temporal resolution (on the order of ~10 sec) and high spatial

279   resolution.

280   **Advantages of PARIS over existing techniques**

10

281 First, PARIS relies solely on light and therefore is virtually non-invasive

282 compared with existing methods including paired-recording(Bennett et al., 1963;

283 Furshpan and Potter, 1959), dye microinjection(Stewart, 1978) and scrape

284 loading (el-Fouly et al., 1987). In addition, given that the activation of the

285 actuator can be specific to subcellular resolution, PARIS can provide spatial

286 information of the functional gap junctions, as shown by our ability to

287 functionally map gap junctions formed at dendrite-dendrite contacts in AL but

288 not at axon-axon contacts in LH between ePNs and iPNs in the *Drosophila*

289 olfactory system (Figure 5), while such resolution cannot be easily achieved by

290 any of the previously existed method.

291 With respect to those relatively non-invasive methods which rely on the

292 diffusion of small fluorescent dyes across gap junctions such as FRAP (Wade

293 et al., 1986) and LAMP (Dakin et al., 2005), a significant advantage of PARIS

294 is that it is fully reversible and does not require the delivery of exogenous dyes.

295 PARIS may serve as a robust tool for screening existing and newly developed

296 gap junction blockers and/or modulators, including clinically relevant

297 compounds such as inhibitors of PKC signaling. In addition, PARIS could

298 possibly be applied to study the dynamic regulation of gap junctions *in vivo*,

299 such as the formation and break of gap junction connections during brain

300 development (Arumugam et al., 2005).

301 Moreover, the actuator and receiver proteins in PARIS are both genetically

302 encoded. Recently, several innovative hybrid approaches were developed to

303 monitor gap junctions (Kang and Baker, 2016; Qiao and Sanes, 2015; Tian et

304 al., 2012). Using a channel/transporter/enzyme-dependent step for the transfer

305 of small molecules, these approaches can in principle achieve genetic

306 specificity in terms of targeting defined cells. In practice, however, these

307 methods require the addition of an exogenous substrate (Qiao and Sanes, 2015;

308 Tian et al., 2012) or a patch electrode to establish an electrochemical gradient

309 between connected cells (Kang and Baker, 2016), thereby limiting their

11

310   application, particularly *in vivo*. In contrast, all of the components in PARIS are

311   genetically encoded by relatively small genes, vastly increasing the range of

312   cell types in which they can be selectively expressed. For example, we show

313   that the PARIS proteins can be introduced using transfection (Figures 1-3),

314   virus-mediated expression (Figure 3), and *ex vivo* transgenic labeling (Figures

315   4 & 5). Given that similar transgenic tools are available for higher organisms,

316   including mammals, PARIS can easily be adapted to other preparations and

317   animal models, including the highly complex mammalian nervous system. In

318   mammalian systems and model organisms in which transgenic techniques are

319   currently unavailable or impractical, recombinant viruses such as lentiviruses,

320   retroviruses, and adeno-associated viruses can be conveniently packaged with

321   these genetic components and used to infect the appropriate target cells.

322   **Limitations of PARIS**

323   In most animal cells, intracellular pH is believed to be tightly regulated for

324   optimal biochemical reactions; thus, even a small change in intracellular pH is

325   rapidly restored to a set point by buffers and proton exchangers/transporters

326   located on the membrane of cells or intracellular organelles (Hoffmann and

327   Simonsen, 1989). This robust system for maintaining pH homeostasis enabled

328   us to repeatedly elicit a PARIS signal in both cultured cells and transgenic

329   animals. One caveat to our approach may be the ability of pH to regulate gap

330   junction activity during PARIS. The uncoupling effect of acidic intracellular pH

331   on GJC has long been described across different Cx consisted gap junctions

332   while alkalization was reported to increase the junctional conductance and the

333   total number of opened channels in gap junction plagues (Palacios-Prado et al.,

334   2010;Turin and Warner, 1977). For the mostly wide expressed Cx43 channels,

335   it has a pKa of ~6.7 in oocytes and fully closed when pH is under 6.4 while fully

336   open when pH is above 7.2 (Peracchia, 2004), which enables PARIS

337   measurement to reveal the GJC mediated by Cx43. However, there is one type

338   of gap junctions that has been reported to be sensitive to alkalization—Cx36

339 consisted gap junctions (Gonzalez-Nieto et al., 2008). Based on the reported

340 pH-conductance curve, the junctional conductance decreased to 50% when pH

341 increase 0.8 unit from 7.2 to 8. As shown in Figure 1–figure supplement 4, 0.1-

342 unit pH increase from 7.35 to 7.45 was enough to induce PARIS signal. So

343 PARIS is still possible in reporting Cx36 consisted GJC under proper activation

344 of the actuator. An even more sensitive pH indicator could help us minimize the

345 pH influence.

346 As we have demonstrated, PARIS is powerful as a genetic tool to map gap

347 junction connections between targeted neurons in the complex central nervous

348 system (Figure 4 & 5). To map unknown gap junctions, firstly we need anatomic

349 information about the two group of cells that we concern to make sure they are

350 spatially contacted, which could be achieved by immunostaining or EM. As the

351 intensive efforts have been or being made to create whole brain connectomes

352 from *C.elegans* (Jarrell et al., 2012), *Drosophila* (FlyEM project, janelia) to

353 zebra fish (Hildebrand et al., 2017) and mice (Allen Mouse Brain Connectivity

354 Atlas), PARIS could utilize these information and databases and possibly help

355 creating electrical connectome.

356 Lastly, PARIS requires the exclusive expression of the actuator and receiver in

357 different cells. Such genetic tools specifically labeling two distinct groups of

358 cells from different cell types or two subgroups from one cell type, might not be

359 accessible in mammals. However, this limitation can be overcome by the

360 intersectional non-overlapping expression of the actuator and receiver, for

361 example using flp-out system. By fusing the receiver with a flippase, the frt

362 sequence flanked actuator would not express in the presence of the receiver.

363 Meanwhile the receiver and the actuator can both designed to be turned on in

364 a cre-dependent manner. This design could make PARIS more versatile in

365 detecting GJC between different cell types labeled by two cre-lines or within the

366 same cell type labeled by one cre-line, without the contamination of the

367 autonomous signal.

13

Future perspectives

Future refinements to PARIS include the use of the new actuators we have screened combining a receiver with higher pH sensitivity, thereby increasing both the signal-to-noise ratio and temporal resolution, allowing for an even wider range of *in vitro* and *in vivo* applications. Finally, the use of additional spectrally non-overlapping pairs of proton-related actuators and receivers, as well as developing actuator-receiver pairs that transport and detect other gap junction–permeable small molecules, may provide the opportunity to detect gap junctions between multiple cell types and/or structures.

ACKNOWLEDGMENTS

AUTHOR CONTRIBUTIONS

Y.L. conceived and supervised the project. Y.L. and L.W. wrote the draft of the manuscript. L.W. performed most of the experiments and data analysis. A.D. performed the electrophysiology experiments and contributed to the data

14

395 analysis and interpretation. L.T.D performed some of the experiments

396 regarding HEK293T cells and contributed to the data analysis and

397 interpretation. S.Q.W. supervised the experiments using cardiomyocytes. All

398 authors contributed to the writing of the manuscript.

399

400 **DECLARATION OF INTERESTS**

401 The authors declare no competing interests.

402
403

404 **REFERENCES**

405

406 Arumugam, H., Liu, X., Colombo, P.J., Corriveau, R.A., and Belousov, A.B. (2005). NMDA
407 receptors regulate developmental gap junction uncoupling via CREB signaling. Nat Neurosci *8*,
408 1720-1726.

409 Belousov, A.B., and Fontes, J.D. (2013). Neuronal gap junctions: making and breaking
410 connections during development and injury. Trends in neurosciences *36*, 227-236.

411 Bennett, M., Aljure, E., Nakajima, Y., and Pappas, G.D. (1963). Electrotonic junctions between
412 teleost spinal neurons: electrophysiology and ultrastructure. Science *141*, 262-264.

413 Bennett, M.V., and Zukin, R.S. (2004). Electrical coupling and neuronal synchronization in the
414 Mammalian brain. Neuron *41*, 495-511.

415 Bhargava, Y., Hampden-Smith, K., Chachlaki, K., Wood, K.C., Vernon, J., Allerston, C.K.,
416 Batchelor, A.M., and Garthwaite, J. (2013). Improved genetically-encoded, FlincG-type
417 fluorescent biosensors for neural cGMP imaging. Frontiers in molecular neuroscience *6*, 26.

418 Butterweck, A., Gergs, U., Elfgang, C., Willecke, K., and Traub, O. (1994). Immunochemical
419 characterization of the gap junction protein connexin45 in mouse kidney and transfected human
420 HeLa cells. The Journal of membrane biology *141*, 247-256.

421 Chen, T.W., Wardill, T.J., Sun, Y., Pulver, S.R., Renninger, S.L., Baohan, A., Schreiter, E.R.,
422 Kerr, R.A., Orger, M.B., Jayaraman, V.*, et al.* (2013). Ultrasensitive fluorescent proteins for
423 imaging neuronal activity. Nature *499*, 295-300.

424 Connors, B.W. (2012). Tales of a dirty drug: carbenoxolone, gap junctions, and seizures.
425 Epilepsy currents *12*, 66-68.

426 Dakin, K., Zhao, Y., and Li, W.H. (2005). LAMP, a new imaging assay of gap junctional
427 communication unveils that Ca2+ influx inhibits cell coupling. Nat Methods *2*, 55-62.

428 Dong, A., Liu, S., and Li, Y. (2018). Gap Junctions in the Nervous System: Probing Functional
429 Connections Using New Imaging Approaches. Frontiers in Cellular Neuroscience *12*.

430 Dubnau, J., Chiang, A.S., Grady, L., Barditch, J., Gossweiler, S., McNeil, J., Smith, P., Buldoc,
431 F., Scott, R., Certa, U.*, et al.* (2003). The staufen/pumilio pathway is involved in Drosophila
432 long-term memory. Curr Biol *13*, 286-296.

15

433   el-Fouly, M.H., Trosko, J.E., and Chang, C.C. (1987). Scrape-loading and dye transfer. A rapid
434   and simple technique to study gap junctional intercellular communication. Exp Cell Res *168*,
435   422-430.
436   Furshpan, E., and Potter, D. (1959). Transmission at the giant motor synapses of the crayfish.
437   The Journal of physiology *145*, 289-325.
438   Gao, S., Nagpal, J., Schneider, M.W., Kozjak-Pavlovic, V., Nagel, G., and Gottschalk, A. (2015).
439   Optogenetic manipulation of cGMP in cells and animals by the tightly light-regulated guanylyl-
440   cyclase opsin CyclOp. Nat Commun *6*, 8046.
441   Garcia-Dorado, D., Inserte, J., Ruiz-Meana, M., González, M.A., Solares, J., Juliá, M., Barrabés,
442   J.A., and Soler-Soler, J. (1997). Gap junction uncoupler heptanol prevents cell-to-cell
443   progression of hypercontracture and limits necrosis during myocardial reperfusion. Circulation
444   *96*, 3579-3586.
445   Gibson, D.G., Young, L., Chuang, R.Y., Venter, J.C., Hutchison, C.A., 3rd, and Smith, H.O.
446   (2009). Enzymatic assembly of DNA molecules up to several hundred kilobases. Nat Methods
447   *6*, 343-345.
448   Gonzalez-Nieto, D., Gomez-Hernandez, J.M., Larrosa, B., Gutierrez, C., Munoz, M.D., Fasciani,
449   I., O'Brien, J., Zappala, A., Cicirata, F., and Barrio, L.C. (2008). Regulation of neuronal
450   connexin-36 channels by pH. Proceedings of the National Academy of Sciences of the United
451   States of America *105*, 17169-17174.
452   Guindon, S., and Gascuel, O. (2003). A simple, fast, and accurate algorithm to estimate large
453   phylogenies by maximum likelihood. Syst Biol *52*, 696-704.
454   Han, X., Chow, B.Y., Zhou, H., Klapoetke, N.C., Chuong, A., Rajimehr, R., Yang, A., Baratta,
455   M.V., Winkle, J., and Desimone, R. (2011). A high-light sensitivity optical neural silencer:
456   development and application to optogenetic control of non-human primate cortex. Frontiers in
457   systems neuroscience *5*.
458   Hildebrand, D.G.C., Cicconet, M., Torres, R.M., Choi, W., Quan, T.M., Moon, J., Wetzel, A.W.,
459   Scott Champion, A., Graham, B.J., Randlett, O.*, et al.* (2017). Whole-brain serial-section
460   electron microscopy in larval zebrafish. Nature *545*, 345-349.
461   Hoffmann, E.K., and Simonsen, L.O. (1989). Membrane mechanisms in volume and pH
462   regulation in vertebrate cells. Physiological reviews *69*, 315-382.
463   Huang, J., Zhang, W., Qiao, W., Hu, A., and Wang, Z. (2010). Functional connectivity and
464   selective odor responses of excitatory local interneurons in Drosophila antennal lobe. Neuron
465   *67*, 1021-1033.
466   Ito, K., Sass, H., Urban, J., Hofbauer, A., and Schneuwly, S. (1997). GAL4-responsive UAS-tau
467   as a tool for studying the anatomy and development of the Drosophila central nervous system.
468   Cell and tissue research *290*, 1-10.
469   Jarrell, T.A., Wang, Y., Bloniarz, A.E., Brittin, C.A., Xu, M., Thomson, J.N., Albertson, D.G., Hall,
470   D.H., and Emmons, S.W. (2012). The connectome of a decision-making neural network.
471   Science *337*, 437-444.
472   Jongsma, H.J., and Wilders, R. (2000). Gap junctions in cardiovascular disease. Circulation
473   research *86*, 1193-1197.
474   Kang, B.E., and Baker, B.J. (2016). Pado, a fluorescent protein with proton channel activity can
475   optically monitor membrane potential, intracellular pH, and map gap junctions. Scientific reports
476   *6*.

16

477 Klapoetke, N.C., Murata, Y., Kim, S.S., Pulver, S.R., Birdsey-Benson, A., Cho, Y.K., Morimoto,
478 T.K., Chuong, A.S., Carpenter, E.J., Tian, Z.*, et al.* (2014). Independent optical excitation of
479 distinct neural populations. Nat Methods *11*, 338-346.

480 Kralj, J.M., Douglass, A.D., Hochbaum, D.R., Maclaurin, D., and Cohen, A.E. (2012). Optical
481 recording of action potentials in mammalian neurons using a microbial rhodopsin. Nature
482 methods *9*, 90-95.

483 Kumar, N.M., and Gilula, N.B. (1996). The gap junction communication channel. Cell *84*, 381-
484 388.

485 Laird, D.W. (2005). Connexin phosphorylation as a regulatory event linked to gap junction
486 internalization and degradation. Biochimica et biophysica acta *1711*, 172-182.

487 Laird, D.W. (2010). The gap junction proteome and its relationship to disease. Trends in cell
488 biology *20*, 92-101.

489 Lampe, P.D. (1994). Analyzing phorbol ester effects on gap junctional communication: a
490 dramatic inhibition of assembly. J Cell Biol *127*, 1895-1905.

491 Langlois, S., Cowan, K.N., Shao, Q., Cowan, B.J., and Laird, D.W. (2008). Caveolin-1 and -2
492 interact with connexin43 and regulate gap junctional intercellular communication in
493 keratinocytes. Molecular biology of the cell *19*, 912-928.

494 Liang, L., Li, Y., Potter, C.J., Yizhar, O., Deisseroth, K., Tsien, R.W., and Luo, L. (2013).
495 GABAergic projection neurons route selective olfactory inputs to specific higher-order neurons.
496 Neuron *79*, 917-931.

497 Miesenbock, G., De Angelis, D.A., and Rothman, J.E. (1998). Visualizing secretion and
498 synaptic transmission with pH-sensitive green fluorescent proteins. Nature *394*, 192.

499 Nihei, O.K., Fonseca, P.C., Rubim, N.M., Bonavita, A.G., Lyra, J.S., Neves-dos-Santos, S., de
500 Carvalho, A.C., Spray, D.C., Savino, W., and Alves, L.A. (2010). Modulatory effects of cAMP
501 and PKC activation on gap junctional intercellular communication among thymic epithelial cells.
502 BMC cell biology *11*, 3.

503 Parnas, M., Lin, A.C., Huetteroth, W., and Miesenbock, G. (2013). Odor discrimination in
504 Drosophila: from neural population codes to behavior. Neuron *79*, 932-944.

505 Paznekas, W.A., Karczeski, B., Vermeer, S., Lowry, R.B., Delatycki, M., Laurence, F., Koivisto,
506 P.A., Van Maldergem, L., Boyadjiev, S.A., and Bodurtha, J.N. (2009). GJA1 mutations, variants,
507 and connexin 43 dysfunction as it relates to the oculodentodigital dysplasia phenotype. Human
508 mutation *30*, 724-733.

509 Peracchia, C. (2004). Chemical gating of gap junction channels; roles of calcium, pH and
510 calmodulin. Biochimica et biophysica acta *1662*, 61-80.

511 Pfeiffer, B.D., Truman, J.W., and Rubin, G.M. (2012). Using translational enhancers to increase
512 transgene expression in Drosophila. Proceedings of the National Academy of Sciences of the
513 United States of America *109*, 6626-6631.

514 Potter, C.J., Tasic, B., Russler, E.V., Liang, L., and Luo, L. (2010). The Q system: a repressible
515 binary system for transgene expression, lineage tracing, and mosaic analysis. Cell *141*, 536-
516 548.

517 Qiao, M., and Sanes, J.R. (2015). Genetic Method for Labeling Electrically Coupled Cells:
518 Application to Retina. Frontiers in molecular neuroscience *8*, 81.

519 Sankaranarayanan, S., De Angelis, D., Rothman, J.E., and Ryan, T.A. (2000). The use of
520 pHluorins for optical measurements of presynaptic activity. Biophysical journal *79*, 2199-2208.

17

521 Shang, Y., Claridge-Chang, A., Sjulson, L., Pypaert, M., and Miesenbock, G. (2007). Excitatory
522 local circuits and their implications for olfactory processing in the fly antennal lobe. Cell *128*,
523 601-612.

524 Shen, Y., Rosendale, M., Campbell, R.E., and Perrais, D. (2014). pHuji, a pH-sensitive red
525 fluorescent protein for imaging of exo-and endocytosis. J Cell Biol *207*, 419-432.

526 Shibayama, J., Paznekas, W., Seki, A., Taffet, S., Jabs, E.W., Delmar, M., and Musa, H. (2005).
527 Functional characterization of connexin43 mutations found in patients with oculodentodigital
528 dysplasia. Circulation research *96*, e83-91.

529 Sirnes, S., Kjenseth, A., Leithe, E., and Rivedal, E. (2009). Interplay between PKC and the
530 MAP kinase pathway in Connexin43 phosphorylation and inhibition of gap junction intercellular
531 communication. Biochem Biophys Res Commun *382*, 41-45.

532 Sohl, G., Maxeiner, S., and Willecke, K. (2005). Expression and functions of neuronal gap
533 junctions. Nature reviews Neuroscience *6*, 191-200.

534 Stewart, W.W. (1978). Functional connections between cells as revealed by dye-coupling with
535 a highly fluorescent naphthalimide tracer. Cell *14*, 741-759.

536 Stocker, R.F., Heimbeck, G., Gendre, N., and de Belle, J.S. (1997). Neuroblast ablation in
537 Drosophila P[GAL4] lines reveals origins of olfactory interneurons. Journal of neurobiology *32*,
538 443-456.

539 Subach, O.M., Gundorov, I.S., Yoshimura, M., Subach, F.V., Zhang, J., Gruenwald, D.,
540 Souslova, E.A., Chudakov, D.M., and Verkhusha, V.V. (2008). Conversion of red fluorescent
541 protein into a bright blue probe. Chemistry & biology *15*, 1116-1124.

542 Tian, L., Yang, Y., Wysocki, L.M., Arnold, A.C., Hu, A., Ravichandran, B., Sternson, S.M.,
543 Looger, L.L., and Lavis, L.D. (2012). Selective esterase-ester pair for targeting small molecules
544 with cellular specificity. Proceedings of the National Academy of Sciences of the United States
545 of America *109*, 4756-4761.

546 Wade, M.H., Trosko, J.E., and Schindler, M. (1986). A fluorescence photobleaching assay of
547 gap junction-mediated communication between human cells. Science *232*, 525-528.

548 Wang, J.W., Wong, A.M., Flores, J., Vosshall, L.B., and Axel, R. (2003). Two-photon calcium
549 imaging reveals an odor-evoked map of activity in the fly brain. Cell *112*, 271-282.

550 Wang, K., Gong, J., Wang, Q., Li, H., Cheng, Q., Liu, Y., Zeng, S., and Wang, Z. (2014). Parallel
551 pathways convey olfactory information with opposite polarities in Drosophila. Proceedings of
552 the National Academy of Sciences *111*, 3164-3169.

553 Yaksi, E., and Wilson, R.I. (2010). Electrical coupling between olfactory glomeruli. Neuron *67*,
554 1034-1047.

555 Zhang, Z., Curtin, K.D., Sun, Y.A., and Wyman, R.J. (1999). Nested transcripts of gap junction
556 gene have distinct expression patterns. Journal of neurobiology *40*, 288-301.

557

558 **MATERIALS AND METHODS**

559 *Key resources table*

Reagent type (species) or resource	Designation	Source or reference	Identifiers	Additional information
Genetic reagent (Drosophila melanogaster)	GH146-Gal4	Liqun LUO lab	RRID:BDSC_30026	
Genetic reagent (Drosophila melanogaster)	GH146-QF	Liqun LUO lab	RRID:BDSC_30015	
Genetic reagent (Drosophila melanogaster)	GH298-Gal4	Liqun LUO lab	RRID:BDSC_37294	
Genetic reagent (Drosophila melanogaster)	Krasavietz-Gal4	Donggen LUO lab	flybaseID#_FBti0027494	
Genetic reagent (Drosophila melanogaster)	ShakB^2	Donggen LUO lab	flybaseID#_FBal0015575	
Genetic reagent (Drosophila melanogaster)	Mz699-Gal4	Liqun LUO lab	flybaseID#_FBti0007260	
Genetic reagent (Drosophila melanogaster)	Repo-Gal4	Yi RAO lab	RRID:BDSC_7415	
Genetic reagent (Drosophila melanogaster)	MB247-Gal4	Yi RAO lab	RRID:BDSC_64306	
Chemical compound,drug	CBX	Sigma-Aldrich	Cat#C4790	
Chemical compound,drug	Heptanol	J&K Scientific	Cat#415422	
Chemical compound,drug	Forskolin	TargetMol	Cat#T2939	

19

Chemical compound,drug	8-Br-cAMP	Sigma-Aldrich	Cat#B7880	
Chemical compound,drug	TPA	Sigma-Aldrich	Cat#P1585	
Chemical compound,drug	Calcein-AM	AAT Bioquest	Cat#22002	
Chemical compound,drug	Fluo-8-AM	AAT Bioquest	Cat#21082	
Recombinant DNA reagent	pcDNA3.1 vector	Micheal LIN lab	Addgene: 52519	
Recombinant DNA reagent	pcDNA3.1-ArchT-BFP2	This study		
Recombinant DNA reagent	pcDNA3.1-pHluorinCAAX	This study		
Recombinant DNA reagent	pcDNA3.1-ArchTD95N-BFP2	This study		
Recombinant DNA reagent	pcDNA3.1-pHluorin	This study		
Recombinant DNA reagent	pcDNA3.1-ArchT-P2A-mRuby3	This study		
Recombinant DNA reagent	pcDNA3.1-mTagBFP-pHluorinCAAX	This study		
Recombinant DNA reagent	pcDNA3.1-BecyclOp-mRuby3	This study		
Recombinant DNA reagent	pcDNA3.1-Cschrimson-mRuby3	This study		
Recombinant DNA reagent	pcDNA3.1-GCamp6SCAAX	This study		
Recombinant DNA reagent	pcDNA3.1-FlincGCAAX	This study		

20

Recombinant DNA reagent	pHuji-P2A-GJA1	This study		
Recombinant DNA reagent	pHuji-P2A-GJA1R202H	This study		
Recombinant DNA reagent	pHuji-P2A-GJA1R76H	This study		
Recombinant DNA reagent	pJFRC28	(Pfeiffer et al., 2012)	Addgene: 36431	
Recombinant DNA reagent	pJFRC28-10xUAS-pHluorinCAAX-p10	This study		
Recombinant DNA reagent	pJFRC28-5xQUAS pHluorinCAAX-p10	This study		
Recombinant DNA reagent	pJFRC28-10xUAS--ArchT-P2A-mRuby3CAAX-p10	This study		
Recombinant DNA reagent	pJFRC28-5xQUAS -ArchT-P2A-mRuby3CAAX-p10	This study		
Full-length human cDNAs	human ORFeome 8.1	Center for Cancer Systems Biology	http://horfdb.dfci.harvard.edu/	
Software, algorithm	ImageJ	NIH	https://imagej.nih.gov/ij/; RRID:SCR_003070	
Software, algorithm	Origin 9.1	OriginLab	https://www.originlab.com/	
Software, algorithm	MATLAB	MathWorks	https://www.mathworks.com/products/matlab.html; RRID:SCR_001622	

21

Other	Inverted confocal microscope	Nikon	Ti-E A1	

560

Molecular cloning

All plasmids were constructed using the Gibson assembly(Gibson et al., 2009)

method. In brief, plasmid vectors and inserts were amplified by PCR using

~30-bp overlapping primers. The fragments were assembled using T5

exonuclease, Phusion DNA polymerase, and Taq DNA ligase (New England

Biolabs). All sequences were verified using Sanger sequencing in our in-

house facility (sequencing platform in the School of Life Sciences of the

Peking University). For cultured cell expression experiments, genes were

cloned into the pcDNA3.1 vector unless otherwise noted. ArchT was amplified

from pAAV-CAG-ArchT-GFP (Han et al., 2011), codon-optimized rhodopsin

genes from different species were synthesized by Qinglan Biotec then fused

at the C-terminus with BFP2, a trafficking sequence (TS), and an ER export

sequence (ERex), producing Actuator-BFP2. In addition, ArchT was linked

directly with a TS and ERex and then fused with mRuby3, yielding pcDNA3.1-

ArchT-P2A-mRuby3. mTagBFP was fused to the N-terminus of pHluorinCAAX

to generate pcDNA3.1-mTagBFP-pHluorinCAAX. The *GJA1* gene was

amplified from a cDNA library (hORFeome database 8.1) and fused with RFP

(pHuji) (Shen et al., 2014)via a P2A linker to generate pHuji-P2A-GJA1, which

was then cloned into the N3 expression vector. Mutations in ArchT and GJA1

were introduced using overlapping PCR with primers containing the mutations

of interest. To generate transgenic *Drosophila* lines, the following four

plasmids were used: ArchT (linked with mRuby3CAAX, HA tag and Flag tag:

ArchT-HA-TS-ERex-P2A-mRuby3-Flag-CAAX) and pHluorinCAAX were

cloned into pJFRC28-10xUAS vector (Pfeiffer et al., 2012)/pJFRC28-5xQUAS

vector (made by replacing 10xUAS with 5XQUAS in pJFRC28) respectively,

22

586   yielding UAS/QUAS-ArchT and UAS/QUAS-pHluorin transgenic flies.

587

588   ***Cell culture and transfection***

589   HEK293T cells and HeLa cells were cultured in DMEM containing 10% (v/v)

590   FBS and 1% penicillin-streptomycin (all from Gibco) at 37°C in humidified air

591   containing 5% CO_2. For transfection, cells were plated at 50% confluence on

592   12-mm glass coverslips in 24-well plates; 12-24 h after plating, the cells were

593   transfected using polyethylenimine (PEI), with a typical ratio of 1 μg DNA : 3 μg

594   PEI per well; 6 h after transfection (or 2 h after transfection for

595   electrophysiological experiments), the culture medium was replaced with fresh

596   medium and the cells were incubated for an additional 18-24 h prior to imaging

597   or electrophysiological recording. For PARIS transfection, the ArchT-BFP2 and

598   pHluorinCAAX constructs were transfected in separate wells; 6 h after

599   transfection, the cells were dissociated, mixed by pipette, combined into a

600   single well, and incubated for 24 h prior to imaging. Alternatively, in some

601   experiments we used sequential transfection, in which the cells were first

602   transfected with the pHluorinCAAX construct; 6 h later, the medium was

603   changed and the cells were transfected with the ArchT-BFP2 construct. The

604   medium was changed 6 h later, and the cells were incubated for 24 h prior to

605   imaging.

606   For PARIS measurements in HeLa cells, 0.5 μg pHluorinCAAX was mixed with

607   0.5 μg pHuji-P2A-GJA1 (or the R202H or R76H mutant version) and transfected

608   into the cells; 10 h later, the medium was replaced with new medium and the

609   cells were transfected with 0.5 μg ArchT-BFP2 mixed with 0.5 μg pHuji-P2A-

610   GJA1 (or the R202H or R76H mutant version). The medium was replaced 10 h

611   later, and the cells were incubated for an additional 24 h prior to imaging.

612   ***pH calibration in HEK293T cells***

23

613 HEK293T cells were co-transfected with the mTagBFP-pHluorinCAAX and

614 ArchT-P2A-mRuby3 plasmids (each at 0.5 µg per well in a DNA:PEI ratio of 1:3)

615 or mTagBFP-pHluorinCAAX alone (1 µg per well) 24 h prior to imaging. Cover

616 slips with cells attached were immersed in Tyrode's solution containing (in mM):

617 150 NaCl, 4 KCl, 2 $MgCl_2$, 2 $CaCl_2$, 10 HEPES, and 10 glucose (pH 7.4) and

618 then pre-treated with 10 µM Nigericin for 5 min, after which the calibration

619 buffers were perfused into the chamber. After Nigericin was added, GFP and

620 BFP channels were recorded simultaneously at 5-s intervals (500 ms/frame,

621 512x512 pixels) using a Nikon A1 confocal microscope. Calibration buffers

622 (containing 10 µM Nigericin) at pH 7, 7.5, 8, 8.5, and 9.5 contained (in mM) 120

623 KCl, 30 NaCl, 2 $MgCl_2$, 10 Glucose, and 10 HEPES; for pH 5.5 and 6.5 buffers,

624 HEPES was replaced with 10 mM MES.

625 ***Electrophysiology***

626 Patch-clamp recordings were performed using an Olympus IX81 upright

627 microscope equipped with a 40x/0.95 NA objective; images were acquired

628 using Micro-Manager (https://micro-manager.org/). Laser light was delivered

629 via a Sutter DG-4 equipped with a xenon lamp. Cultured HEK293T cells were

630 bathed in Tyrode's solution. Actuator HEK293T cells were identified by blue

631 fluorescence (excitation filter: 350/50 nm; emission filter: 448/60 nm). ArchT

632 was activated using the same light source filtered through a 560/25-nm Sutter

633 VF5 filter. Light intensity was adjusted using the Sutter DG-4 and was

634 calculated by measuring the light power transmitted through the objective using

635 a SANWA laser power meter LP1). Recording electrodes (with a tip resistance

636 of 3-6 MΩ when filled with internal solution) were fabricated using a Sutter P-

637 97 electrode puller and controlled using Sutter MP-225 micromanipulators. The

638 recording electrodes were filled with an internal solution containing (in mM): 130

639 K-gluconate, 10 KCl, 2 $MgCl_2$, 2.5 Mg-ATP, 0.25 Na-GTP, 10 HEPES, and 0.4

640 EGTA (pH adjusted to 7.4 with KOH; osmolarity adjusted to 300 mOsm with

641 sucrose); where indicated, 100 µM carbenoxolone (CBX) (Sigma-Aldrich) was

24

642   applied by perfusion. The recording signal was amplified and digitized using a

643   HEKA EPC10 double patch-clamp amplifier and collected using Patch Master.

644   Currents were smoothed using a 20-ms moving average in order to minimize

645   50 Hz AC noise. For simultaneous optical and electrophysiology recordings, the

646   Sutter DG-4 light source was triggered by the HEKA EPC10 amplifier in order

647   to synchronize the electrophysiological recording with the light simulation. All

648   recordings were performed at room temperature.

649   ***FRAP measurements in HEK293T cells***

650   A 1 mM stock solution of Calcein-AM was added to the culture medium to a

651   final concentration of 1 μM. The cells were then incubated for 10 min before

652   washing 3 times with 1 ml Tyrode's solution. The coverslips containing the

653   attached cells were then placed in a chamber containing Tyrode's solution and

654   imaged using a Nikon A1 confocal microscope. A typical FRAP experiment was

655   performed using 488 nm imaging for measuring the baseline (1 sec/frame, 5-

656   sec interval, 5 frames, 512x512 pixels), 405 nm bleaching (12 sec, ROI ~5 μm

657   in diameter within the cell), and 488 nm imaging for 2 min in order to track

658   Calcein recovery.

659   ***Preparation, culture, transfection, and infection of primary***
660   ***cardiomyocytes***

661   Cardiomyocytes (CMs) were enzymatically dissociated from the ventricles of

662   neonatal (P0) Sprague-Dawley rats, and 0.5-1$\times$10^5 CMs per well were seeded

663   on 12-mm glass coverslips coated with poly-D-lysine (Sigma-Aldrich) in 24-well

664   plates and grown in DMEM containing 10% FBS and 1% penicillin-streptomycin

665   (all from Gibco) at 37°C in humidified air containing 5% CO_2. Forty-eight hours

666   after plating, CMs were simultaneously transfected with the ArchT-BFP2

667   plasmids using Lipofectamine 3000 (Invitrogen) and infected with an

668   adenovirus carrying pHluorinCAAX under CMV promoter (Vigene Biosciences).

669   In brief, before transfection/infection, the medium in each well was replaced

25

670 with 500 µl Opti-MEM. DNA (1 µg) and Lipofectamine 3000 (1.5 µl) were diluted

671 in 100 µl Opti-MEM and incubated for 15 min at room temperature before

672 additional to each well. At the same time, 1 µl of adeno-associated virus

673 carrying the pHluorinCAAX ($3x10^{10}$ pfu/ml) was added into the same wells.

674 Eight hours later, the Opti-MEM was replaced with standard DMEM medium,

675 and the CMs were incubated for an additional 24 h prior to imaging.

Measurements of beating rate and Ca^{2+} transients in CMs

677 CMs were transfected with ArchT-BFP2 plasmids using Lipofectamine 3000 as

678 described above; 24 h after transfection, CMs expressing ArchT-BFP2 were

679 loaded with 1 µM Fluo-8 AM (AAT Bioquest) for 20 min, washed with 1 ml

680 Tyrode's solution for three times. CMs were imaged with 488 nm excitation in

681 Tyrode's solution at room temperature using a Nikon A1 confocal microscope

682 for 1 min to record Ca^{2+} transients, followed by stimulation with 561 nm for 20

683 sec (5 trials at 2 min intervals). After stimulation, another 1 min of time-lapse

684 imaging was performed using 488 nm excitation to record Ca^{2+} transients. Ca^{2+}

685 transients recorded before and after light stimulation were counted using

686 ImageJ analysis of the green channel. All images were generated at a rate of

687 100 ms/frame. Beating rate was measured using ImageJ analysis of the white-

688 field images.

Fly strains

690 *Drosophila* stocks were raised at 25°C on standard corn meal-agar-molasses

691 medium. GH298-Gal4, Mz699-Gal4 (III) (Ito et al., 1997), and GH146-Gal4 (II)

692 (Stocker et al., 1997) and GH146-QF(Potter et al., 2010) were kindly provided

693 by Dr. Liqun Luo. Krasavietz-Gal4 (Dubnau et al., 2003) and ShakB^2 (Zhang et

694 al., 1999) strains were gifts from Dr. Donggen Luo. Repo-Gal4 and MB247-Gal4

695 strains were gifts from Dr. Yi RAO. UAS/QUAS-ArchT and UAS/QUAS-

696 pHluorinCAAX transgenic flies were generated at the Core Facility of

697 *Drosophila* Resource and Technology, Institute of Biochemistry and Cell Biology,

26

698   Chinese Academy of Sciences.

Ex vivo fly brain preparations for PARIS imaging

700   The entire brain from adult flies within 2 weeks after eclosion was dissected

701   using fine forceps into Ca^{2+}-free adult-like hemolymph (ALH) containing (in mM):

702   108 NaCl, 5 KCl, 5 HEPES, 5 trehalose, 5 sucrose, 26 $NaHCO_3$, 1 NaH_2PO_4, 2

703    $CaCl_2$, and 1-2 $MgCl_2$ (275 mOsm) (Wang et al., 2003). The brain was then

704   transferred to a glass-bottom chamber containing ALH for confocal imaging.

705   The brain was held in place using a custom-made platinum frame and

706   positioned with the anterior surface of the brain toward the objective (for

707   imaging and stimulation of the antennal lobe), or with the posterior surface

708   toward the objective (for imaging and stimulation of the lateral horn).

Fluorescence imaging and light stimulation

710   Imaging and light stimulation were performed using an inverted Nikon A1

711   confocal microscope equipped with a Nikon sapphire laser and either a

712   40x/1.35 NA oil objective (for HEK293T and HeLa cells) or a 20x/0.75 NA air

713   objective (for CMs and fly brains). During imaging, the cells (HEK293T cells,

714   HeLa cells, or CMs) were immersed in Tyrode's solution. Cells expressing the

715   actuator (ArchT-BFP2) or receiver (pHluorinCAAX) were identified by the

716   presence of blue or green fluorescence respectively. ArchT-BFP2 was excited

717   at 405 nm and visualized using a 450/50-nm filter; pHluorin was excited at 488

718   nm and visualized using a GaSP photomultiplier after passing through a

719   525/50-nm filter. Blue fluorescent cells in adjacent to green cells were selected

720   to conduct photostimulation with a ROI of 10-20 μm in diameter. ArchT was

721   photostimulated using a 561 nm scanning laser at 0.5 mW for experiments

722   using cell lines (except for the power-dependent measurements) and 0.1 mW

723   for experiments using CMs. Typically, cells were first imaged using 488 nm

724   excitation (256x256 pixels, 500 ms/frame, 2-5 sec intervals) to obtain a baseline

725   fluorescence measurement. After obtaining a baseline, pulses of 561 nm laser

27

726 light were applied to activate the ArchT (4 sec/pulse, 5-10 pulses with no delay),

727 intertwined with 488 nm imaging of the receiver. The 488 nm imaging was

728 continued (2-5 sec intervals) for 1-2 min after the 561-nm stimulation in order

729 to record the fluorescence recovery of the receiver. For experiments using gap

730 junction blockers and modulators, 100 µM CBX (Sigma-Aldrich), 2 mM heptanol

731 (J&K Scientific), 500 µM 8-Br-cAMP (Sigma-Aldrich), 500 µM forskolin

732 (TargetMol), or 340 nM TPA (Sigma-Aldrich) was applied by adding a 1000x

733 stock solution to the chamber. For CM experiments, heptanol was washed out

734 of the chamber for 3 min by perfusion with Tyrode's solution.

735 Fly brains were stimulated and imaged in ALH using the same laser

736 configuration described above. The antennal lobe (AL) and lateral horn (LH)

737 were identified by the presence of pHluorin fluorescence and were stimulated

738 with 0.5 mW laser intensity using an ROI 20-30 µm in diameter.

739 ***Data analysis***

740 Time series images were analyzed using Nikon NIS and ImageJ with a batch-

741 registration plugin (Nimmerjahn et al., 2009). A mean background value

742 obtained from regions away from the pHluorin was subtracted in order to correct

743 for fluorescence intensity (F). For each pixel, we calculated the normalized

744 change in fluorescence intensity ($\Delta F/F_0$), where F_0 is the baseline fluorescence

745 averaged from 5 frames obtained prior to light stimulation. $\Delta F/F_0$ over time was

746 further processed using Origin 9.1 (OriginLab). $\Delta F/F_0$ images were processed

747 with MATLAB (MathWorks) using custom-written scripts in order to produce

748 pseudocolor images.

749 ***Data presentation and statistical analysis***

750 All summary data are reported as the mean ± s.e.m. Differences between

751 groups were tested using the Student's unpaired or paired *t*-test, and

752 differences with $p < 0.05$ (two-sided) were considered statistically significant.

753

28

754   **FIGURE LEGENDS**

755

756   **Figure 1. The principle behind PARIS and proof-of-concept in cultured**
757   **cells by PARIS based on ArchT and pHluorin .**

758   (A) Schematic diagram depicting the principle and process of PARIS. (B1-B3)
759   Demonstration of PARIS using in HEK293T cells. (B1) Schematic depicting the
760   principle of ArchT/pHluorin pair based PARIS. (B2), Representative images
761   showing expression of the actuator ArchT-BFP (blue) and the receiver
762   pHluorinCAAX (green) in transfected HEK293T cells neighboring to each other.
763   The pseudocolor images showing the basal fluorescence and 4-sec ArchT
764   activation induced pHluorin response in the adjacent cell/remote cell. (B3),
765   Representative traces and group analysis of $\Delta F/F_0$ in the cells adjacent and
766   remote to the actuator cells (n=10-17 cells). The stimulus (561nm light, 0.5 mW)
767   is indicated by the yellow circle in the image and the yellow vertical line in the
768   traces. (C1-C3) Similar to (B), except PARIS signals were recorded before and
769   after CBX treatment (100 µM, n=10 cells). (D) Representative traces of $\Delta F/F_0$
770   using increasing stimulation time (laser power, 0.5 mW). (E-F) Grouped peak
771    $\Delta F/F_0$ and peak signal-to-noise ratio (SNR) of PARIS signals recorded with
772   increasing stimulation time (n=5-12 cells for each data point); the data were fit
773   to a single Hill function (solid lines). (G) Summary of the half-rise and half-decay
774   times of the PARIS signals measured with 4-sec or 20-sec stimulation (n=14-
775   18 cells).
776   The scale bars represent 10 µm.
777   *p<0.05, **p<0.01, ***p<0.001, N.S., not significant (p>0.05).
778   In this and subsequent figures, error bars in the representative traces indicate
779   the s.e.m. from 3 repeat experiments.

780

781   **Figure 2. PARIS's validation by electrophysiological recording and its**
782   **comparison with FRAP in HEK293T cells..**

783   (A1-A2) PARIS detection of gap junctional coupling under increasing light
784   power and the application of CBX (0.01 mW to 1.5 Mw, 20 sec). (B1-B2)
785   Electrophysiological recording of the gap junctional currents during actuator
786   activation. (B1), Schematic diagram depicting dual patch-clamp recording of a
787   pair of HEK293T cells connected by gap junctions; one cell of the pair
788   expresses ArchT-BFP. (B2), Light steps applied to the actuator cell (top, from
789   0.1 mW to 0.5 mW), recorded currents in the receiver cell (middle); elimination
790   of the currents by the application of CBX (100 µM, bottom). (C1-C2) Similar
791   experiment using the same cells shown in (B), except that voltage steps (from
792   -60 mV to -40 mV) were applied to the actuator cell, while the receiver cell was
793   clamped at -50 mV. (D1-D3) Input-output curve for peak $\Delta F/F_0$ % or currents
794   measured in the receiver cell versus illumination intensity or voltage in the
795   absence or presence of CBX (100 µM). (E) Summary data showing the relative
29

796 CBX-mediated inhibition of signals measured with PARIS or current recording
797 (n=3-15 cells per group). (F) Schematic depicting the process of FRAP method
798 to detect gap junctional communication using Calcein-AM dye. (G,H)
799 Comparison of basal fluorescence between PARIS and FRAP during sequential
800 five photostimulation and photobleaching. (G) Exemplary images showing the
801 fluorescence of Calcein or pHluorin at the beginning of 1st, 3rd and 5th FRAP or
802 PARIS measurement. (H) Traces of fluorescence intensity from 5 consecutive
803 FRAP and PARIS measurements. The half-rise time for the first traces are
804 indicated with dotted lines reflecting the curve-fit analysis. Yellow or purple lines
805 represent the stimulation (561nm) or bleaching (405nm) period. (I) Quantified
806 comparison of basal fluorescence, SNR and the half-rise time between FRAP
807 and PARIS method as experiments shown in (G,F) (n=5 cells).
808 The scale bar represents 10 μm in (G).
809 ***p < 0.001, N.S., not significant.
810

811 **Figure 3. Use of PARIS to measure GJC in cultured cell lines and primary**
812 **cardiomyocytes.**
813 (A) Top, representative images showing adjacent HEK293T cells expressing
814 ArchT/pHluorin. Bottom, pseudocolor images of 40-sec laser illumination–
815 induced peak PARIS signals in receiver cells. Where indicated, the cells were
816 treated with DMSO (Ctrl), 8-Br-cAMP (500 μM), Forskolin (10 μM), or TPA (340
817 nM) for 6 h before PARIS measurements. (B) Representative traces and group
818 analysis of PARIS signals in (A) (n= 6-8 cells per group). (C) Top, representative
819 images showing expression of ArchT/pHluorin in HeLa cells with or without
820 transfection of various gap junction proteins. Bottom, pseudocolor images of
821 40-sec laser illumination–induced peak PARIS signals measured in receiver
822 cells. (D) Representative traces and group analysis of PARIS signals in (C) (n
823 = 6-10 cells per group). (E) Schematic diagram depicting the application of
824 PARIS in cultured rat cardiomyocytes (CMs). Shown below is a corresponding
825 confocal image of the actuator CM and receiver CM, which express ArchT and
826 pHluorinCAAX, respectively. Note that the actuator CM expresses both ArchT
827 and pHluorinCAAX. (F) Top, PARIS responses in the actuator and receiver CMs.
828 Shown at the left is a confocal image of the actuator and receiver CMs. Bottom,
829 corresponding traces of the experiments shown in a before, during, and 3 min
830 after removal of heptanol (2 mM). Note that the light stimulus elicited a response
831 in both CMs, but only the receiver CM was sensitive to heptanol. (G-H),
832 Summary of the half-rise and half-decay times of the PARIS signals and peak
833 $\Delta F/F_0$ for pHluorinCAAX fluorescence in receiver CMs (n=10 cells)
834 The scale bars represent 10 μm (A,C) or 50 μm (F).
835 *p<0.05, **p<0.01, ***p<0.001, N.S., not significant (p>0.05).
836

837 **Figure 4. Detection of GJC between specific neurons in transgenic**
838 ***Drosophila* by PARIS**
839 (A) Schematic diagram depicting the anatomy of the antennal lobe (AL) in a

30

840　transgenic Drosophila line in which the ePNs express ArchT and the eLNs
841　express pHluorinCAAX (indicated in red and green, respectively). D, V, L, and
842　M refer to dorsal, ventral, medial, and lateral, respectively. (B, C) Pseudocolor
843　images (B) and time course (C) of PARIS signals in the AL of the transgenic
844　flies shown in (A). Note that a 30-sec pulse of 561nm light (0.5 mW) elicited a
845　significant PARIS signal between ePNs and eLNs (top row); in contrast, no
846　signal was elicited when the brain was treated with 100 μM CBX (middle row),
847　in flies with the ShakB[2] mutation (bottom row). (D, E) Pseudocolor images (D)
848　and time course (E) showing PARIS responses of four ROIs from the lateral (L),
849　dorsal (D), middle and ventral (V) part of the AL in the same transgenic
850　*Drosophila* line in (A). Where indicated, the flies were treated with saline or
851　carbenoxolone (CBX); n=5 flies per group. (F, G) Summary of the peak PARIS
852　signal (F) and the half-rise and half-decay times (G) elicited by 30-sec
853　photostimulation (n=7-15 flies per group). (H) Group data for the peak PARIS
854　response between eLNs-ePN measured in the four stimulating ROIs indicated
855　in (D) (n = 5 flies per group).
856　The scale bars 20 μm.
857　Two-sample Student's t-test was performed. **p < 0.005, ***p < 0.001, N.S., not
858　significant.
859

860　**Figure 5. Mapping GJC at specific subcellular structures in transgenic**
861　***Drosophila* by PARIS**
862　(A) Schematic diagrams depicting two transgenic Drosophila lines in which the
863　ePNs express pHluorinCAAX and iPNs express ArchT (top, shown in green and
864　red), or only the iLNs co-expressing ArchT and pHluorinCAAX (bottom, shown
865　in yellow) in the olfactory pathway are indicated. (B, C) Pseudocolor images (B)
866　and time course (C) of PARIS signals in the AL and LH regions of the transgenic
867　flies shown in (A). Note that in flies in which the ePNs and iPNs express the
868　receiver and actuator, respectively, a 20-sec pulse of yellow light elicited a
869　significant PARIS signal in the AL, but not in the LH. Moreover, the signal
870　induced in the AL was inhibited by 100 μM CBX. CBX had no effect in flies in
871　which the actuator and receiver were co-expressed in the same iPNs (i.e., in
872　the cis configuration). (D-F) Group data for the peak PARIS signals (D), the half-
873　rise and half-decay times measured in the indicated conditions (E) and the iPN
874　autonomous responses (n = 3-11 flies per group).
875　The scale bars in (B) represent 20 μm.
876　*p < 0.05, two-sample Student's t-test); N.S., not significant (p > 0.05)
877

878　**Figure 6. Further optimization of PARIS by screening of more potent**
879　**proton actuators.**
880　(A) Screening for high efficiency proton actuators. Actuators were fused with
881　BFP at the C-terminus and co-expressed with pHluorinCAAX in HEK293T cells.
882　Top left, membrane trafficking performance of two candidates besides ArchT;
883　top right, phylogenic tree of screened rodopsins. The tree was built using

31

884 PhyML(Guindon and Gascuel, 2003); bottom, cell-autonomous pHluorin
885 signals of all the potential proton pumps under 20-sec photostimulation (n=5-
886 13 cells per group). (B,C) Exemplary responses and grouped cell-autonomous
887 peak $\Delta F/F_0$ % of ArchT, Lari and CarO under increased laser power (20s
888 stimulation time). The data were fit to a single Hill function (solid lines, n=10
889 cells for each data point).
890 The scale bar in (A) represents 10 μm .
891

SUPPLEMENTARY FIGURE LEGENDS

893

Figure 1–figure supplement 1. Poor performance of actuators and
receivers based on detecting cGMP and Ca^{2+}.
896 (A1-A3) Activation of a GMP photocyclase BeCyclOp induced no detectable
897 fluorescence change in a cGMP sensor FlincG3 in 293T cells co-expressing
898 cGMP based actuator and receiver (561nm, 0.5 mW, 40 s). (B1-B3) Similar to
899 (A) but used an actuator and a receiver based on Ca^{2+} (561nm, 0.5 mW, 80 s).
900 (C-D) Group analysis and comparison of peak $\Delta F/F_0$ % and peak SNR among
901 three pairs of actuator/receiver based on proton, cGMP, Ca^{2+} respectively (n=3-
902 11 cells per group).
903 The scale bars represent 10 μm.
904 N.S., not significant (p > 0.05).
905

Figure 1–figure supplement 2. Functional characterization of actuator
and receiver based on ArchT and pHluorin .
908 (A1-A3) Photostimulation induced increases of pHluorin fluorescence in
909 HEK293T cells co-expressing ArchT and pHluorinCAAX (top row) or pHluorin
910 (second row), but not in HEK293T cells co-expressing ArchTD95N and
911 pHluorinCAAX (third row) or expressing only pHluorinCAAX (bottom row). The
912 stimulus (561nm light, 0.5mW) is indicated by the yellow circle in the image (A2)
913 and shaded area in the traces (A3). Error bars indicate ±SEM from 3 repeats
914 (B) Group data for the experiments shown in (A & B) (n=11-23 cells per group).
915 (C-F) Representative autonomous traces and group peak $\Delta F/F_0$ % under
916 increased stimulating time (0.5mW laser power, C-D) or increased laser power
917 (20s stimulation time, E-F). The lines are single Hill fits to the data (n = 3–10
918 cells for each point).
919 The scale bars represent 10μm.
920 ***$p < 0.001$.
921

Figure 1–figure supplement 3. Probing GJC propagation within
connected HEK293T cells by PARIS
924 (A) Schematic diagram depicting a cluster of four HEK293T cells connected by
925 gap junctions. One cell expresses the actuator, and the three receiver cells (R1,
926 R2, and R3) are connected in series to the actuator. (B,C) Time-lapse
927 pseudocolor images and $\Delta F/F_0$ traces of the PARIS signals measured in the

32

928 receiver cells following light-induced activation of the actuator cell. (D) Group
929 data of the peak change in pHluorinCAAX fluorescence in cells R1, R2, and R3
930 measured as shown in (B); n = 16 cells per group.
931 The scale bar in (B) represents 10 μm.
932 **p < 0.005 and ***p < 0.001.
933

934 **Figure 1–figure supplement 4. Quantification of ArchT activation-**
935 **induced pH change in actuator cells.**
936 (A) Schematic diagram showing the process for calibrating pH. (B) Confocal
937 images showing pHluorin (top) and BFP fluorescence (bottom) of cells perfused
938 with buffers with the indicated pH levels. (C) pH calibration curve for mTagBFP-
939 pHluorinCAAX. The GFP/BFP ratio was fitted with a Hill function (n=10 cells for
940 each point). (D) Schematic diagram and confocal images showing co-
941 expression of mTagBFP-pHluorinCAAX and ArchT-P2A-mRuby3. The yellow
942 circle indicates the stimulation region. (E) Representative traces of the
943 GFP/BFP ratio and pH change upon a 20-sec or 4-sec stimulation at 561 nm (3
944 stimuli delivered at 3-min intervals) in cells co-expressing mTagBFP-
945 pHluorinCAAX and ArchT-P2A-mRuby3 (green lines) and in cells expressing
946 only mTagBFP-pHluorinCAAX (gray line). Error bars indicate the s.e.m. from
947 triplicate experiments. (F) Summary of the estimated peak change in pH in the
948 experiments shown in (E) based on the calibration curve shown in (C) (n=10
949 cells per group).
950 The scale bars represents10 μm.
951 A, actuator cells; R, receiver cells.
952

953 **Figure 3–figure supplement 1. Spontaneous Ca²⁺ transients and beating**
954 **rate in rat cardiomyocytes expressing ArchT.**
955 (A) Example images of a cardiomyocyte (CM) expressing ArchT (left), showing
956 Fluo-8 fluorescence at the rest state (middle) and the exciting state (right). (B)
957 Ca^{2+} transients measured using Fluo-8 fluorescence in the same CM shown in
958 (A) before and after light stimulation. (C-D) Summary of the rate of Ca^{2+}
959 transients measured with Fluo-8 (C) and the beating rates (D) from
960 untransfected CMs and ArchT-expressing CM before and after light stimulation
961 (n=11-26 cells per group); cells were stimulated with 20-sec pulses at 0.1 mW
962 with 2-min intervals for five repeats.
963 The scale bar represents 50 μm.
964 n.s., not significant (p>0.05).
965

966 **Figure 4 – figure supplement 1. Cell-autonomous PARIS signal measured**
967 **in the ePNs of transgenic *Drosophila*.**
968 (A) Schematic diagram depicting the imaging setup and the antennal lobe (AL)
969 in a transgenic fly co-expressing ArchT and pHluorinCAAX in ePNs. (B-D)
970 Pseudocolor images (B), representative traces (C), and summary data (D)
971 showing ePN-autonomous pHluorinCAAX responses measured in the AL (n=6-

972   9 flies per group). Note that the light stimulus had no effect in flies in which
973   ArchT was not expressed. (E) Time course of the change in pHluorin
974   fluorescence in responses to 561-nm light delivered at the indicated power. (F)
975   Laser illumination with 647 nm light at 1 mW does not induce a detectable
976   PARIS signal. (G) Peak $\Delta F/F_0$ plotted against laser power. The solid line is a
977   Hill fit to the data (n=9 for each data point). (H) Repetitive light stimuli elicit a
978   reproducible cell-autonomous signal in transgenic flies. Shown are ten
979   consecutive recordings of ePN signals collected over a 2-hour period; where
980   indicated, 561-nm light was applied at 0.5 mW. The dashed horizontal line
981   indicates the average peak response from the ten stimuli. (I), Summary of the
982   peak change in pHluorinCAAX fluorescence normalized to the first response
983   measured at the indicated times (n=8-13 flies for each group).
984   The scale bar represents 20 μm.
985   ***p<0.001, n.s., not significant (p>0.05).
986
987   **Figure 4 – figure supplement 2. Composite confocal images of dissected**
988   **fly brain expressing actuators and receivers in genetically labeled cells.**
989   Red channel, the expression of RFP (mRuby3) linked ArchT; green channel,
990   the expression of pHluorinCAAX. The correspondent diver lines used were
991   listed on the left side.
992   The scale bars represent 50 μm.
993
994   **Figure 4 – figure supplement 3. No obvious PARIS signal was detected**
995   **from ePN-KC, ePN-iLN and eLN-Glia pairs.**
996   (A-C) Similar to Figure 4, except the PARIS signal was measured between
997   ePNs and Keyon cells (ePN-KC), inhibitory local neurons (ePN-iLN), and glial
998   cells (ePN-Glia); n=7-17 flies per group. PARIS signals between ePNs and
999   eLNs (ePN-eLN) from Figure 4 were represented as a control.
1000 The scale bar represents 20 μm.
1001 ***p<0.001.
1002
1003 **Figure 5 – figure supplement 1. Composite confocal images of dissected**
1004 **fly brain expressing actuators and receivers in iPNs and ePNs.**
1005 Red channel, the expression of RFP (mRuby3) linked ArchT; green channel,
1006 the expression of pHluorinCAAX. The correspondent diver lines used were
1007 listed on the left side.
1008 The scale bar represents 50 μm.
1009
1010 **Figure 6 – figure supplement 1. Membrane traffic performance of two**
1011 **proton-pumps compared with ArchT.**
1012 (A) Confocal images showing the expression of two new proton pumps besides
1013 ArchT in HEK293T cells. Proton pumps were fused with BFP at the C-terminus
1014 and co-expressed with pHluorinCAAX. (B) The normalized line-scanning plots
1015 of the fluorescence signals in both blue and green channels. (C) Relative

34

1016   colocalization were measured by Pearson's colocalization ratios of the
1017   Autuator-BFP according to pHluorinCAAX (n = 28 for each protein).
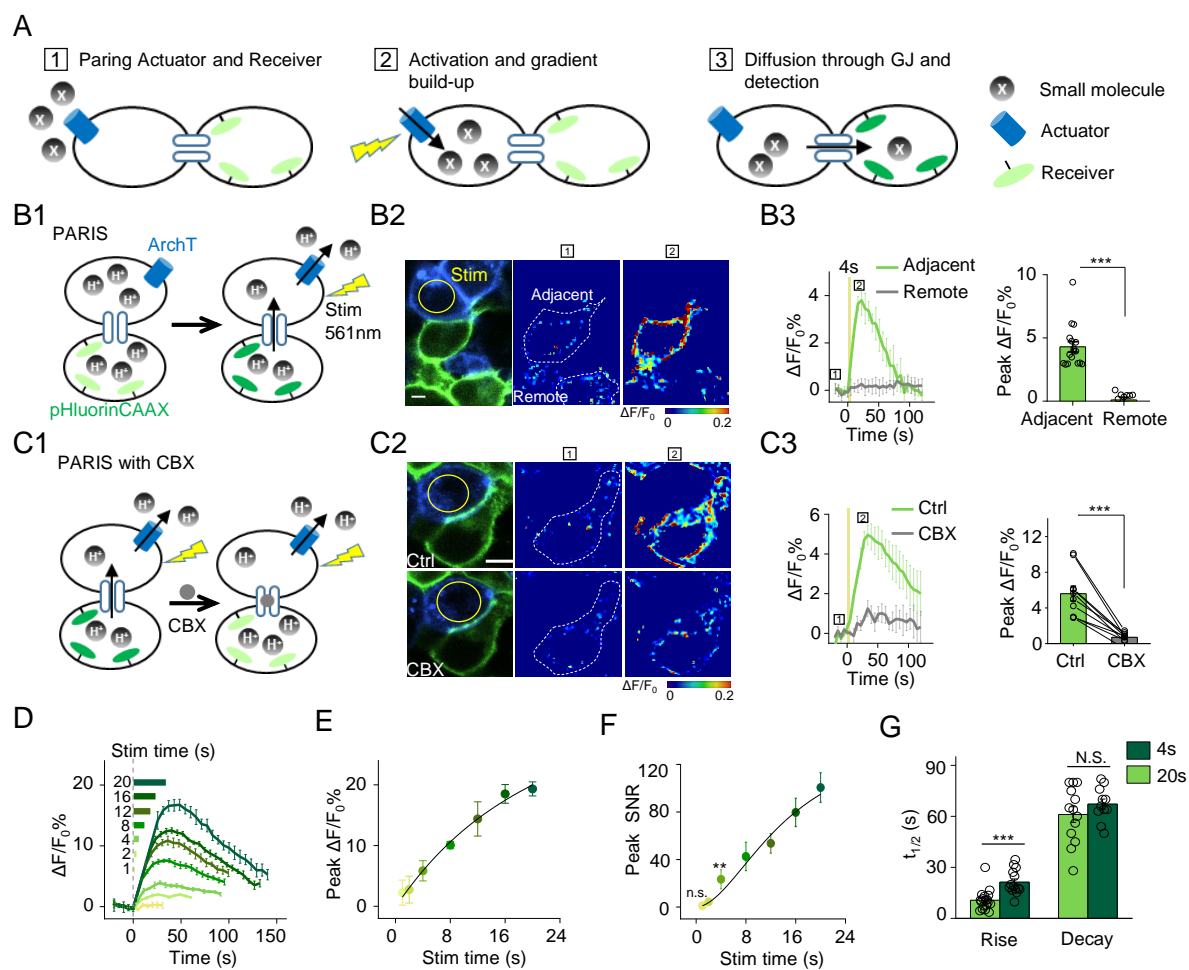1018   The scale bars represent 10 µm.
1019   ***p<0.001.

35

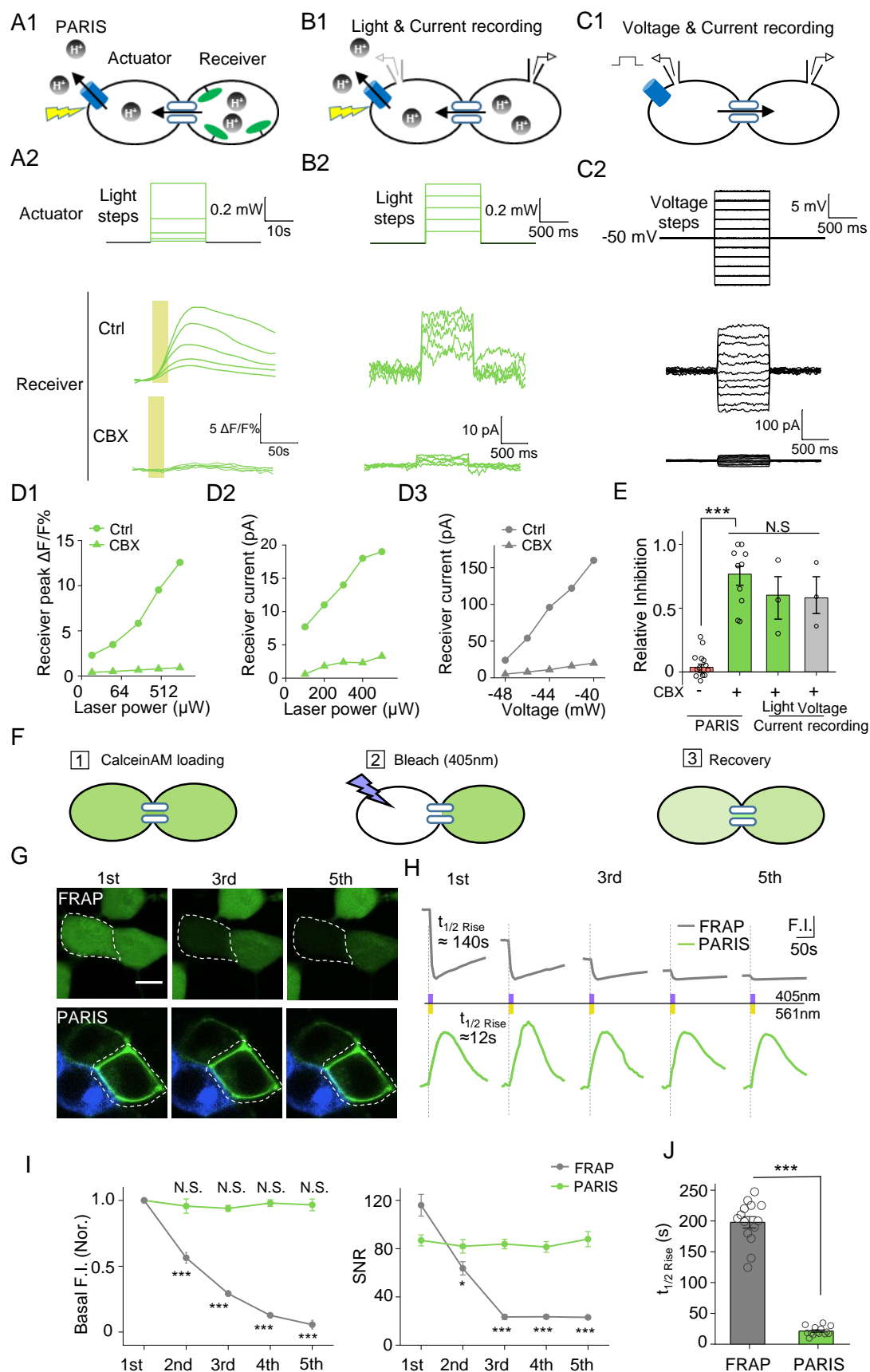**Figure 1. The principle behind PARIS and proof-of-concept in cultured cells by PARIS based on ArchT and pHluorin .**

Figure 2. PARIS's validation by electrophysiological recording and its comparison with FRAP in HEK293T cells.
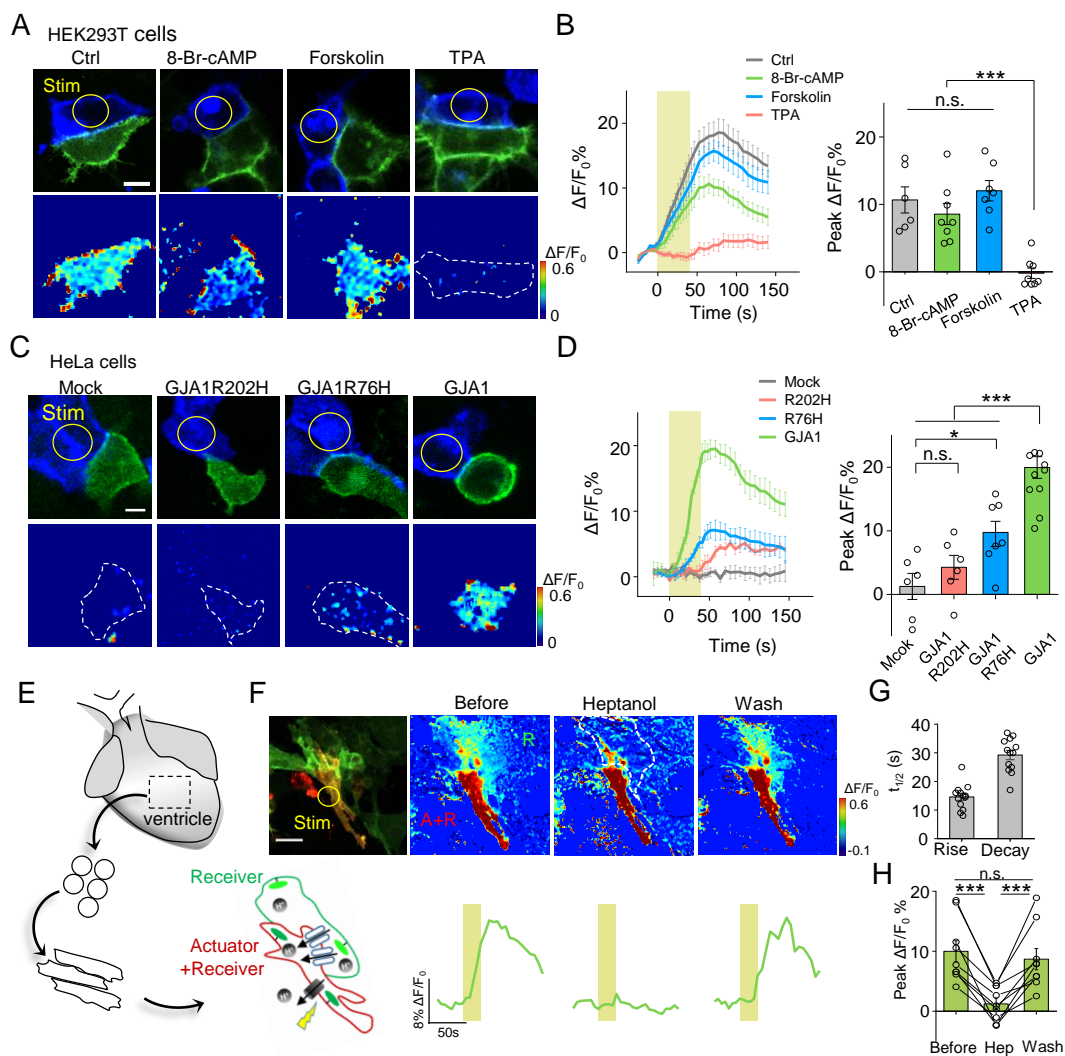
Figure 2. Use of PARIS to measure GJC in cultured cell lines and primary cardiomyocytes.

Figure 4. Detection of GJC between specific neurons in transgenic *Drosophila* by PARIS
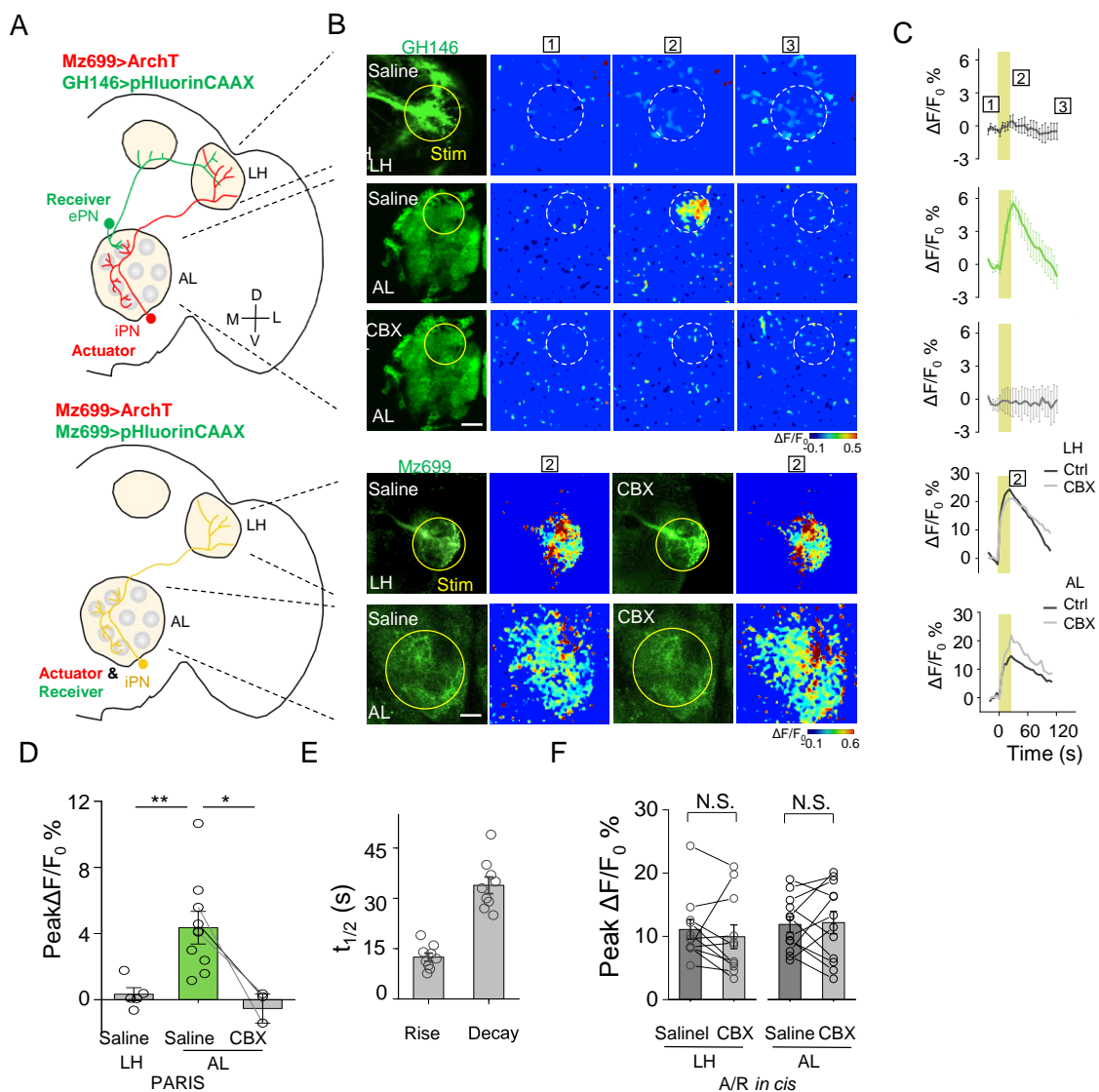
Figure 5. Mapping GJC at specific subcellular structures in *Drosophila* brain by PARIS
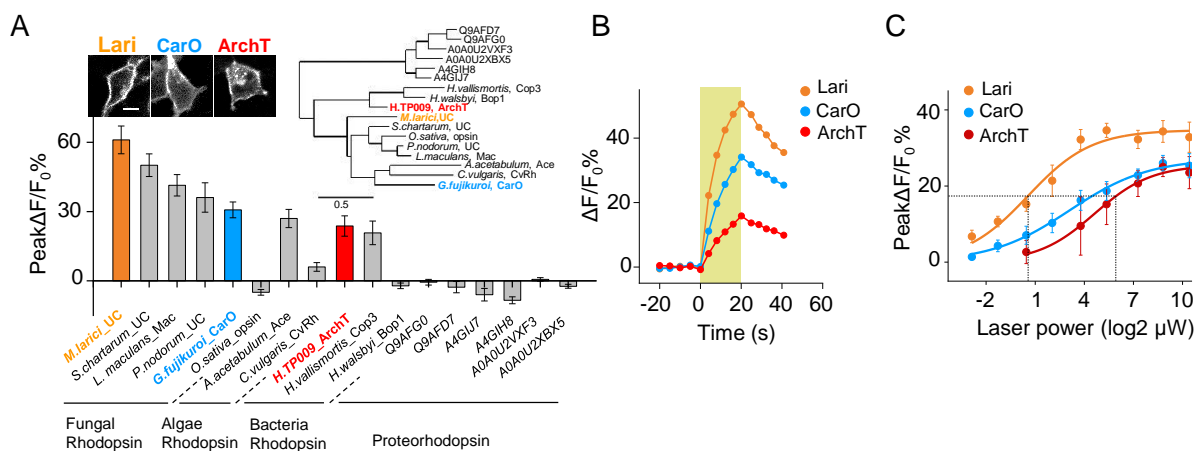
Figure 6. Further optimization of PARIS by screening of more potent proton pumps.
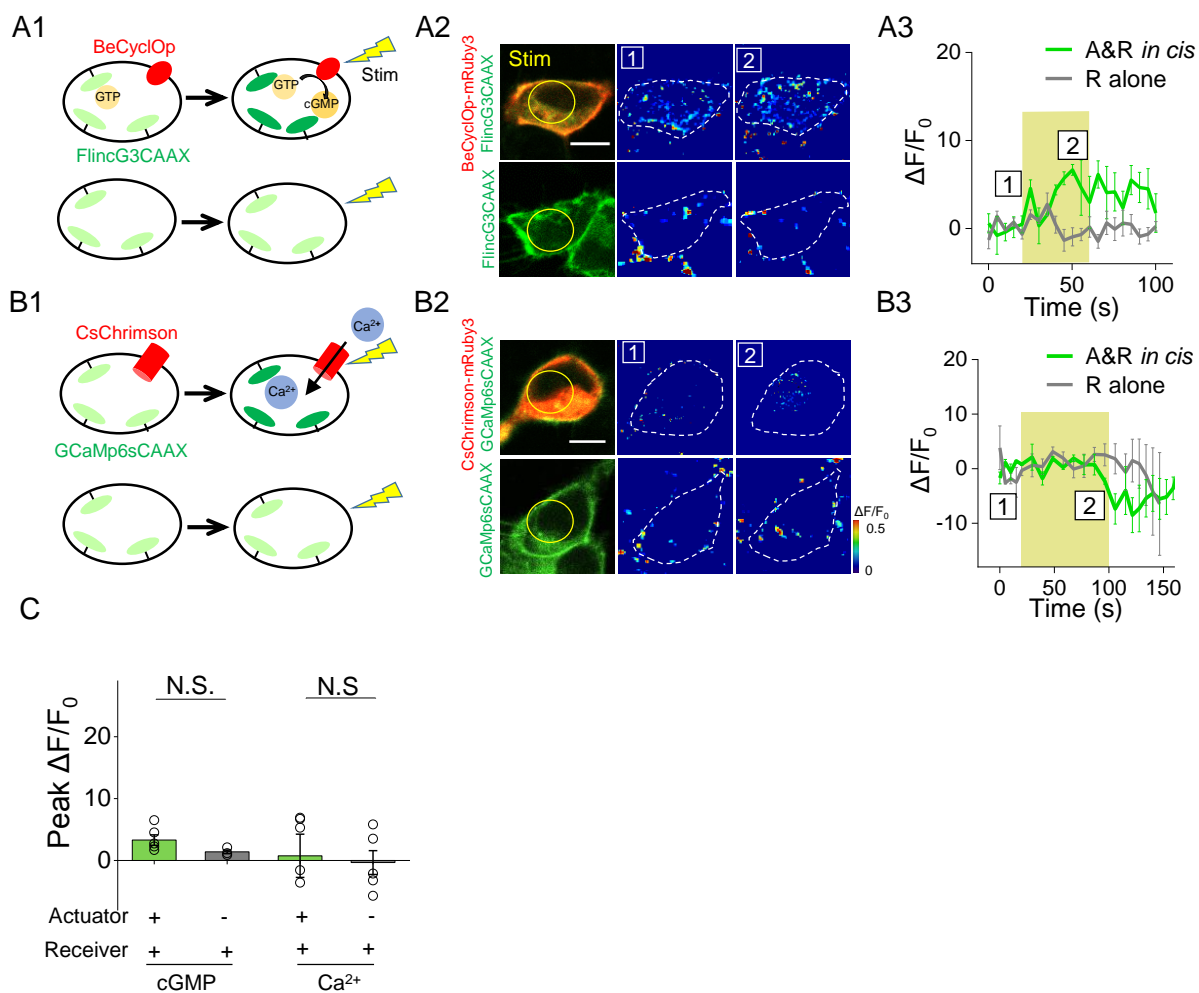
Figure 1–figure supplement 1. Poor performance of actuators and receivers based on detecting cGMP and Ca^{2+} .
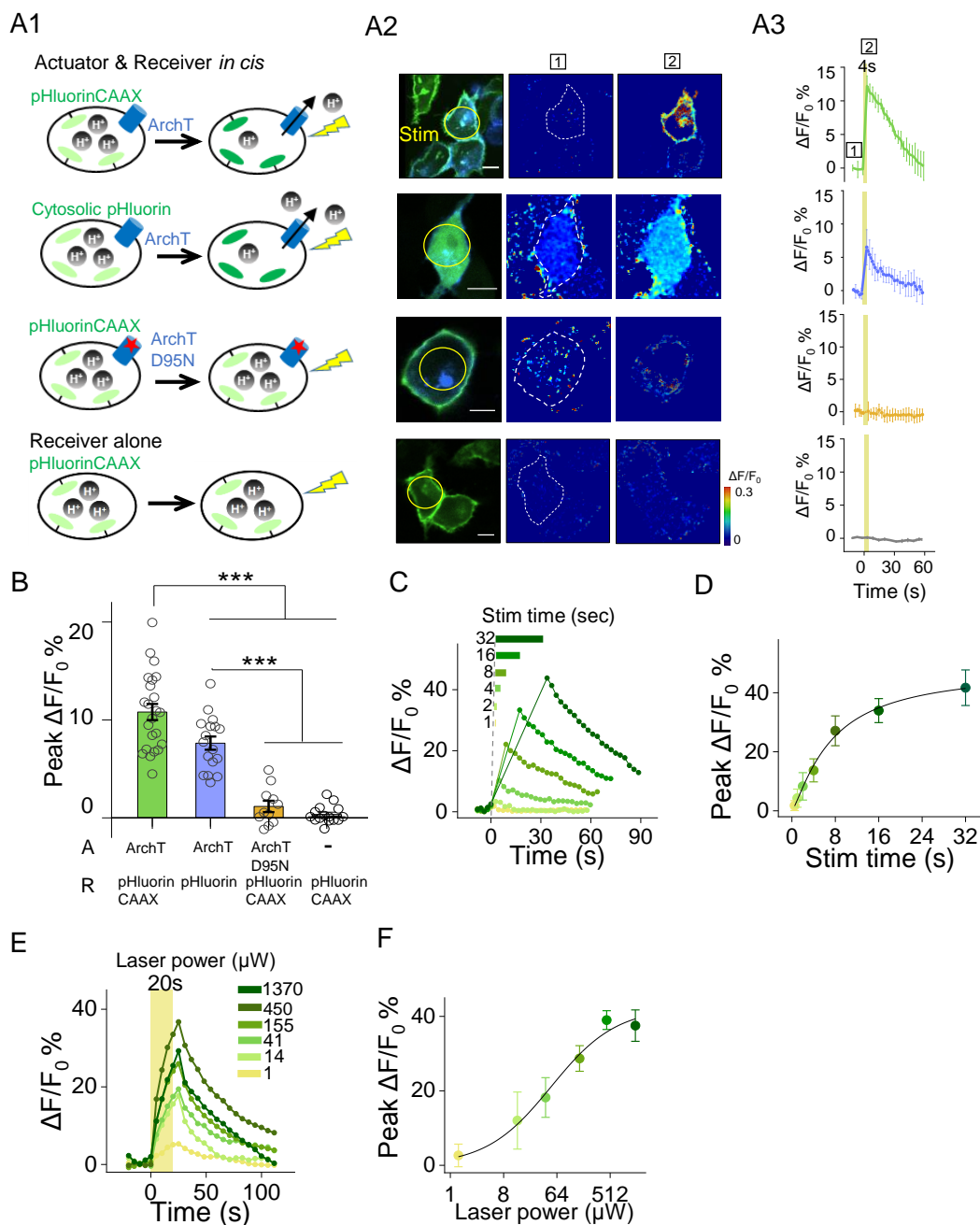
Figure 1–figure supplement 2. Functional characterization of actuator and receiver based on ArchT and pHluorin .
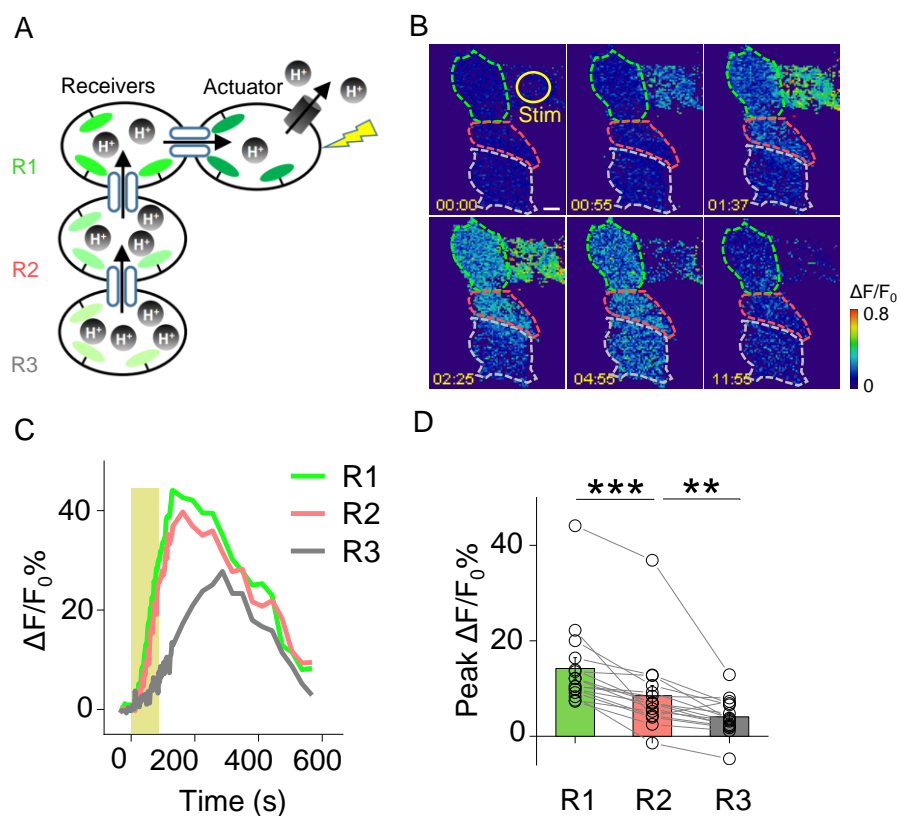
Figure 1–figure supplement 3. Probing GJC propagation within connected HEK293T cells by PARIS
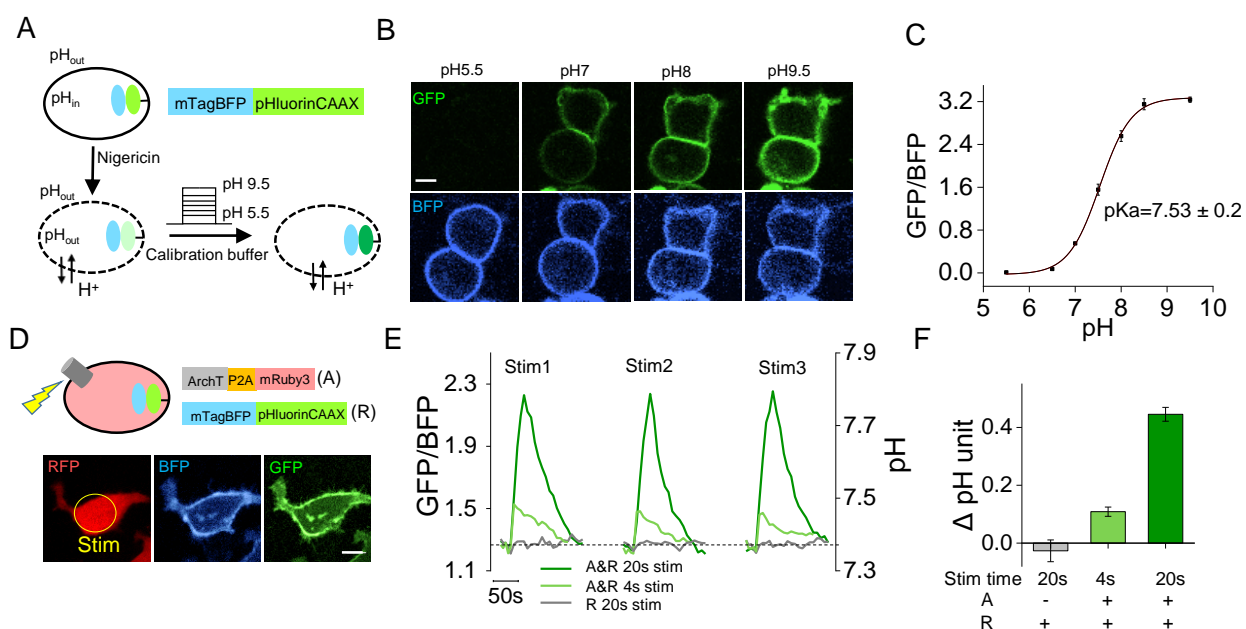
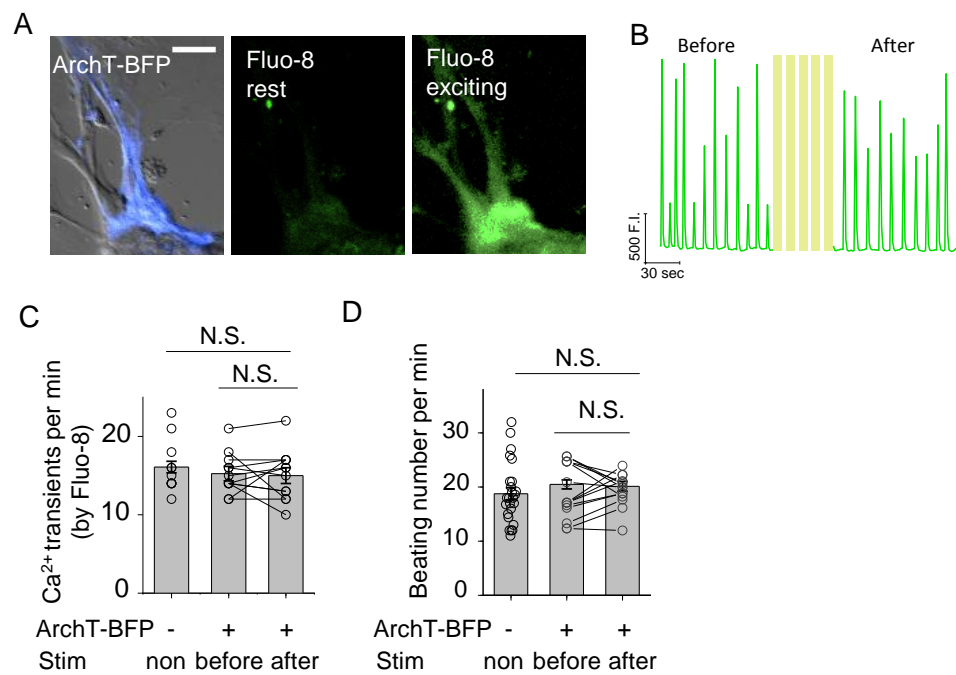**Figure 1–figure supplement 4.** Quantification of ArchT activation-induced pH change in actuator cells.

Figure 3–figure supplement 1. Spontaneous Ca²⁺ transients and beating rate in rat cardiomyocytes expressing ArchT.
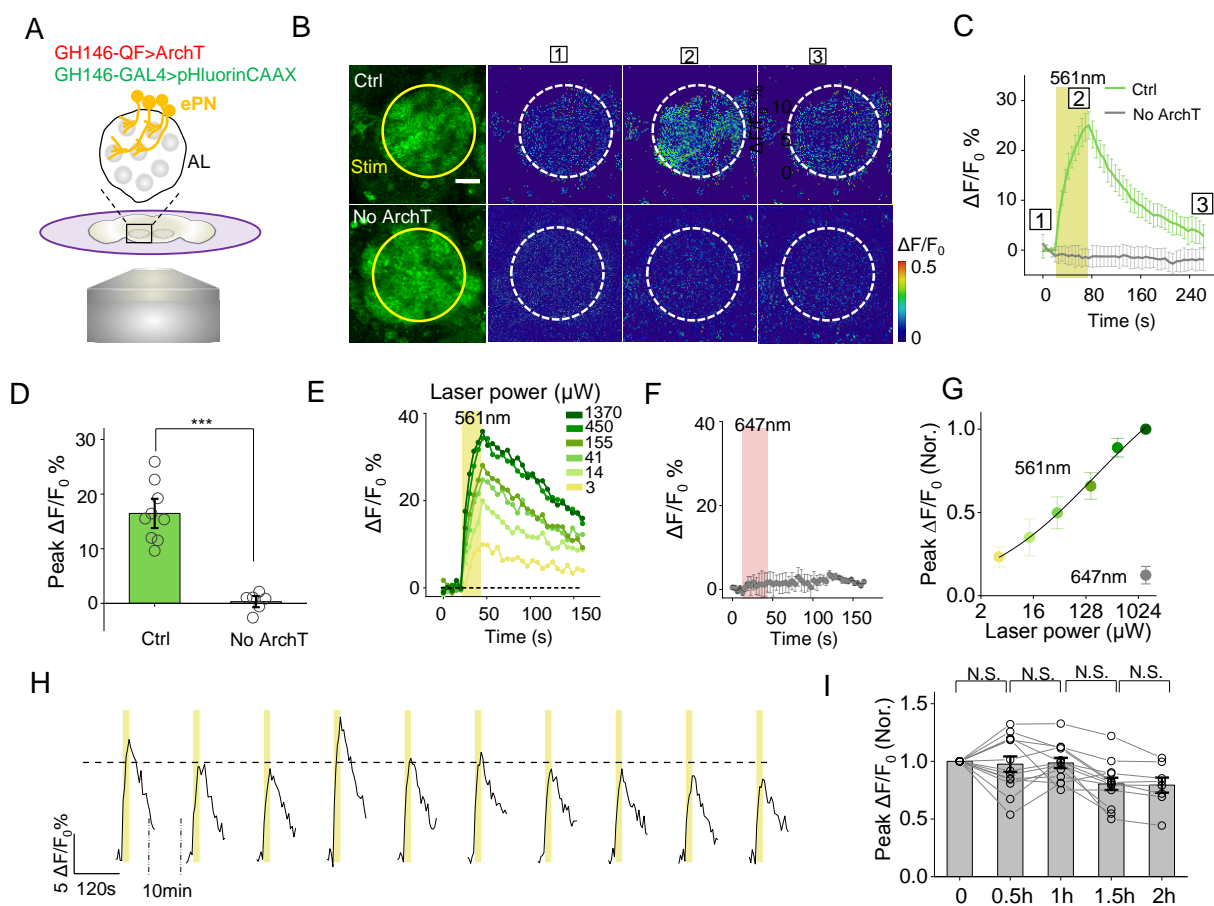
A

GH146-QF>ArchT
GH146-GAL4>pHluorinCAAX

ePN

AL

B

Ctrl
Stim

No ArchT

1   2   3

ΔF/F$_0$
0.5

0

C

561nm

ΔF/F$_0$ %

Ctrl
No ArchT

30

20

10

0

Time (s)
0   80   160   240

D

Peak ΔF/F$_0$ %

***

30

20

10

0

Ctrl   No ArchT

E

Laser power (µW)

561nm

ΔF/F$_0$ %

1370
450
155
41
14
3

40

20

0

Time (s)
0   50   100   150

F

647nm

ΔF/F$_0$ %

40

20

0

Time (s)
0   50   100   150

G

Peak ΔF/F$_0$ (Nor.)

561nm

647nm

1.0

0.5

0.2

Laser power (µW)
2   16   128   1024

H

ΔF/F$_0$ %
5

120s   10min

I

N.S.   N.S.   N.S.   N.S.

Peak ΔF/F$_0$ (Nor.)

1.5

1.0

0.5

0.0

0   0.5h   1h   1.5h   2h

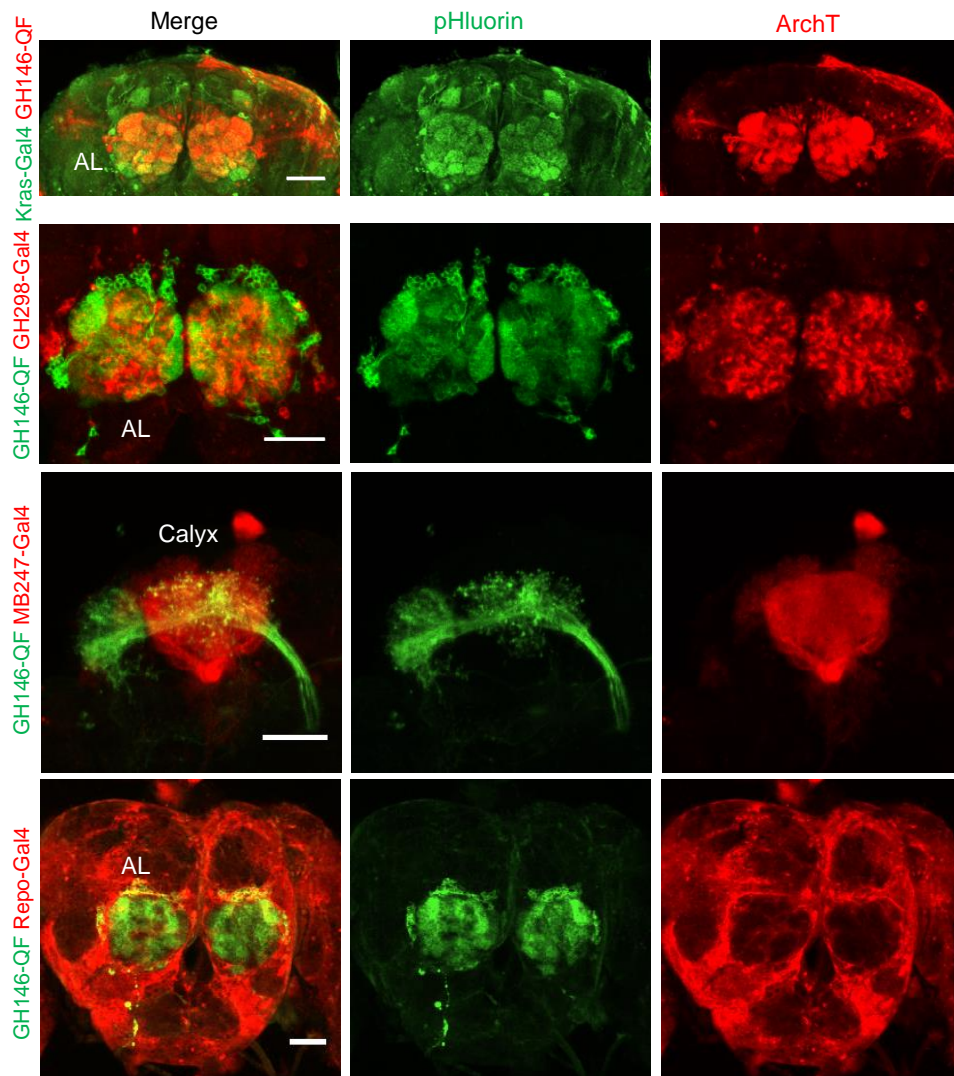**Figure 4 – figure supplement 1. Cell-autonomous PARIS signal measured in the ePNs of transgenic *Drosophila*.**

Figure 4 – figure supplement 2. Composite confocal images of dissected fly brain expressing actuators and receivers in genetically labeled cells.
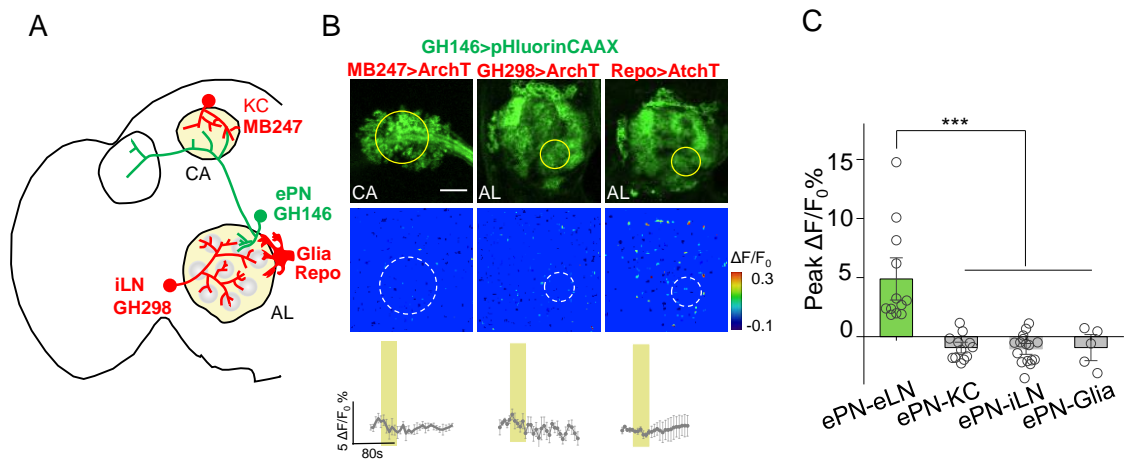
Figure 4 – figure supplement 3. No obvious PARIS signal was detected from ePN-KC, ePN-iLN and eLN-Glia pairs.
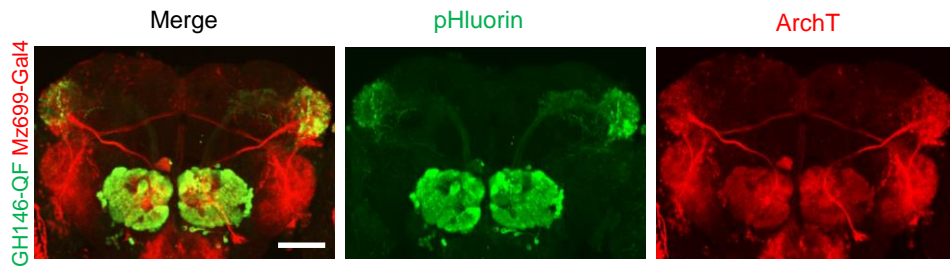
Figure 5 – figure supplement 1. Composite confocal images of dissected fly brain expressing actuators and receivers in iPNs and ePNs.
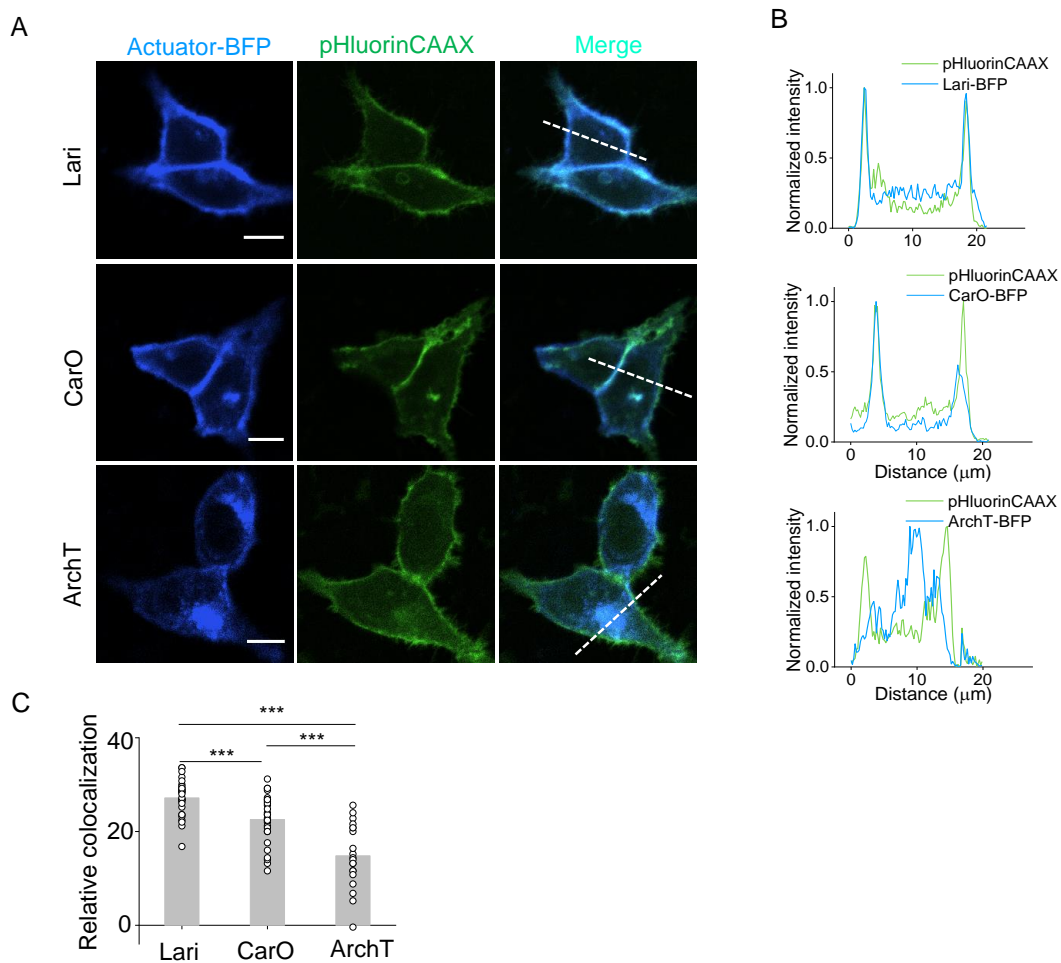
Figure 6 – figure supplement 1. Membrane traffic performance of two proton-pumps compared with ArchT.